# Historical and future changes in air pollutants from CMIP6 models

Steven Turnock, Robert Allen, Martin Andrews, Susanne Bauer, Makoto Deushi, Louisa Emmons, Peter Good, Larry Horowitz, Jasmin John, Martine Michou, et al.

Atmos. Chem. Phys., 20, 14547–14579, 2020
https://doi.org/10.5194/acp-20-14547-2020


Atmospheric Chemistry and Physics
Open Access
EGU

# Historical and future changes in air pollutants from CMIP6 models

**Steven T. Turnock[1], Robert J. Allen[2], Martin Andrews[1], Susanne E. Bauer[3,4], Makoto Deushi[5], Louisa Emmons[6], Peter Good[1], Larry Horowitz[7], Jasmin G. John[7], Martine Michou[8], Pierre Nabat[8], Vaishali Naik[7], David Neubauer[9], Fiona M. O'Connor[1], Dirk Olivié[10], Naga Oshima[5], Michael Schulz[10], Alistair Sellar[1], Sungbo Shim[11], Toshihiko Takemura[12], Simone Tilmes[6], Kostas Tsigaridis[3,4], Tongwen Wu[13], and Jie Zhang[13]**

[1]Met Office Hadley Centre, Exeter, UK
[2]Department of Earth and Planetary Sciences, University of California Riverside, Riverside, CA, USA
[3]Center for Climate Systems Research, Columbia University, New York, NY, USA
[4]NASA Goddard Institute for Space Studies, New York, NY, USA
[5]Meteorological Research Institute, Tsukuba, Japan
[6]Atmospheric Chemistry Observations and Modelling Lab, National Center for Atmospheric Research, Boulder, CO, USA
[7]NOAA Geophysical Fluid Dynamics Laboratory, Princeton, NJ, USA
[8]Centre National de Recherches Météorologiques (CNRM), Université de Toulouse, Météo-France, CNRS, Toulouse, France
[9]Institute of Atmospheric and Climate Science, ETH Zurich, Zurich, Switzerland
[10]Division for Climate Modelling and Air Pollution, Norwegian Meteorological Institute, Oslo, Norway
[11]National Institute of Meteorological Sciences, Seogwipo-si, Jeju-do, Korea
[12]Research Institute for Applied Mechanics, Kyushu University, Fukuoka, Japan
[13]Beijing Climate Center, China Meteorological Administration, Beijing, China

**Correspondence:** Steven T. Turnock (steven.turnock@metoffice.gov.uk)

Received: 30 December 2019 – Discussion started: 21 January 2020
Revised: 1 October 2020 – Accepted: 9 October 2020 – Published: 30 November 2020

**Abstract.** Poor air quality is currently responsible for large impacts on human health across the world. In addition, the air pollutants ozone ($O_3$) and particulate matter less than 2.5 µm in diameter ($PM_{2.5}$) are also radiatively active in the atmosphere and can influence Earth's climate. It is important to understand the effect of air quality and climate mitigation measures over the historical period and in different future scenarios to ascertain any impacts from air pollutants on both climate and human health. The Coupled Model Intercomparison Project Phase 6 (CMIP6) presents an opportunity to analyse the change in air pollutants simulated by the current generation of climate and Earth system models that include a representation of chemistry and aerosols (particulate matter). The shared socio-economic pathways (SSPs) used within CMIP6 encompass a wide range of trajectories in precursor emissions and climate change, allowing for an improved analysis of future changes to air pollutants. Firstly, we conduct an evaluation of the available CMIP6 models against surface observations of $O_3$ and $PM_{2.5}$. CMIP6 models consistently overestimate observed surface $O_3$ concentrations across most regions and in most seasons by up to 16 ppb, with a large diversity in simulated values over Northern Hemisphere continental regions. Conversely, observed surface $PM_{2.5}$ concentrations are consistently underestimated in CMIP6 models by up to 10 µg m$^{-3}$, particularly for the Northern Hemisphere winter months, with the largest model diversity near natural emission source regions. The biases in CMIP6 models when compared to observations of $O_3$ and $PM_{2.5}$ are similar to those found in previous studies. Over the historical period (1850–2014) large increases in both surface $O_3$ and $PM_{2.5}$ are simulated by the CMIP6 models across all regions, particularly over the mid to late 20th century, when anthropogenic emissions increase markedly. Large regional historical changes are simulated for both pollutants across East and South Asia with an annual mean increase of up to 40 ppb for $O_3$ and 12 µg m$^{-3}$ for $PM_{2.5}$. In future scenarios containing strong air quality and climate mitigation measures (ssp126), annual mean concentrations of air pollutants are substantially reduced across all regions by up to 15 ppb for $O_3$ and 12 µg m$^{-3}$ for $PM_{2.5}$. However, for sce-

narios that encompass weak action on mitigating climate and reducing air pollutant emissions (ssp370), annual mean increases in both surface $O_3$ (up 10 ppb) and $PM_{2.5}$ (up to $8\,\mu g\,m^{-3}$) are simulated across most regions, although, for regions like North America and Europe small reductions in $PM_{2.5}$ are simulated due to the regional reduction in precursor emissions in this scenario. A comparison of simulated regional changes in both surface $O_3$ and $PM_{2.5}$ from individual CMIP6 models highlights important regional differences due to the simulated interaction of aerosols, chemistry, climate and natural emission sources within models. The projection of regional air pollutant concentrations from the latest climate and Earth system models used within CMIP6 shows that the particular future trajectory of climate and air quality mitigation measures could have important consequences for regional air quality, human health and near-term climate. Differences between individual models emphasise the importance of understanding how future Earth system feedbacks influence natural emission sources, e.g. response of biogenic emissions under climate change.



## 1 Introduction

Air pollutants are important atmospheric constituents as they have large impacts on human health (Lelieveld et al., 2015), damage ecosystems (Fowler et al., 2009) and can also influence climate through changes in the Earth's radiative balance (Boucher et al., 2013; Myhre et al., 2013). Two major components of air pollution at the surface are ozone ($O_3$) and particulate matter less than 2.5 µm in diameter ($PM_{2.5}$). Exposure to present-day ambient concentrations of these two air pollutants was estimated to cause up to 4 million premature deaths per year (Apte et al., 2015; Malley et al., 2017). Over recent decades, the impact on human health from exposure to air pollutants has been increasing (Butt et al., 2017; Cohen et al., 2017). Additionally, elevated levels of air pollutants over recent decades have also been responsible for ecosystem damage to crops and vegetation, although there have been recent improvements in environmental health (de Wit et al., 2015).

In terms of climate impact, tropospheric $O_3$ has a positive radiative forcing on climate over the industrial period and is the third-most important greenhouse gas in terms of radiative forcing (Myhre et al., 2013). However, depletion of $O_3$ in the stratosphere has resulted in a net negative top-of-atmosphere radiative forcing over recent decades (Checa-Garcia et al., 2018). Particulate matter (PM), also referred to as aerosols, has an overall negative radiative forcing on climate, both directly and indirectly, through the modification of cloud properties (Boucher et al., 2013). Both $O_3$ and PM are relatively short lived in the troposphere, with a typical lifetime of less than 2 weeks in the lower atmosphere, and are commonly referred to as short-lived climate forcers (SLCFs). Future air pollutant concentrations and distributions are driven by changes to both precursor emissions and climate. Emission control measures on both a national and international level can influence future changes to air pollutants, with global increases in $CH_4$ abundance potentially offsetting benefits to surface $O_3$ from local emission reductions (Fiore et al., 2002; Shindell et al., 2012; Wild et al., 2012). For $PM_{2.5}$, changes in concentrations are dependent on both emission rates and levels of atmospheric oxidants, although changes in specific aerosol components can be more directly related to emissions, e.g. black carbon. In a warming world, background $O_3$ concentrations over remote locations are likely to decrease (Johnson et al., 1999; Isaksen et al., 2009; Fiore et al., 2012; Doherty et al., 2013), whereas over anthropogenic source regions, which have higher average surface $O_3$ concentrations, an increase is anticipated (Rasmussen et al., 2013; Colette et al., 2015). The climate impact on $PM_{2.5}$ is much more uncertain and variable across regions, with both increases and decreases predicted due to the uncertainty of future meteorological effects (Jacob and Winner, 2009; Allen et al., 2016; Shen et al., 2017). However, any such climate change impacts on $PM_{2.5}$ are considered to be smaller than the effect from implementing emission mitigation measures (Westervelt et al., 2016).

Experiments conducted as part of the Coupled Model Intercomparison Project Phase 5 (CMIP5; Taylor et al., 2012) and the Atmospheric Chemistry and Climate Model Intercomparison Project (ACCMIP; Lamarque et al., 2013) contributed to a multi-model assessment of future trends in air pollutants. Global annual mean surface $O_3$ concentrations were predicted to increase by up to 5 ppb in 2100 using RCP8.5 (Representative Concentration Pathway with an anthropogenic radiative forcing of $8.5\,W\,m^{-2}$ in 2100), the RCP with the largest increases in methane ($CH_4$) abundances and the largest climate change signal used in CMIP5 (Kirtman et al., 2013). The other RCPs used in CMIP5 had a lower climate forcing and smaller changes in $CH_4$ abundance, with models predicting global annual mean surface $O_3$ concentrations that showed little change in the short term (up to 2050) but decreased by around 5 ppb in 2100. The scenario differences in the global mean response for surface $O_3$ were generally reflected across other regions, al-

though with a larger magnitude of change over the Northern Hemisphere continental regions. The predicted range of future surface $O_3$ concentrations was previously found to be dominated by changes in precursor emissions (Fiore et al., 2012). However, in regions remote from pollution sources (low-$NO_x$), future climate change was shown to result in a small reduction in surface $O_3$ concentrations. For $PM_{2.5}$, results from the CMIP5 and ACCMIP models showed annual mean concentrations declining in most regions and across all scenarios due to the reduction in aerosol emissions. Globally, $PM_{2.5}$ concentrations reduced by $\sim 1\,\mu g\,m^{-3}$ by 2100, whereas larger regional reductions of up to $6\,\mu g\,m^{-3}$ were predicted by 2100. Exceptions to this occurred over South and East Asia, where $PM_{2.5}$ concentrations increased by up to $3\,\mu g\,m^{-3}$ in the near-term (up to 2050), after which concentrations reduced by 2100. The largest difference in the response of $PM_{2.5}$ across the scenarios was also shown across East and South Asia due to differences in the carbonaceous and sulphur dioxide ($SO_2$) emission trajectories (Fiore et al., 2012). Future $PM_{2.5}$ concentrations over Africa and the Middle East were shown to be quite noisy due to the large meteorological variability that influences dust emissions over these regions.

The current set of experiments conducted for the Coupled Model Intercomparison Project Phase 6 (CMIP6; Eyring et al., 2016) represent an opportunity to update the assessment of current and future levels of air pollutants using the latest generation of Earth system and climate models. A new set of future scenarios have been generated for CMIP6: the shared socio-economic pathways (SSPs), which combine different trends in social, economic and environmental developments (O'Neill et al., 2014). Varying amounts of emission mitigation to SLCFs are applied on top of the baseline social and economic developments to meet predefined climate and air quality targets in the future, allowing for a wider range of future air pollutant trajectories to be assessed than what occurred in CMIP5 (Rao et al., 2017; Riahi et al., 2017). Initial assessments have been made of future changes to air pollutants in the SSPs using simplified models (Reis et al., 2018; Turnock et al., 2018, 2019). The sustainability pathway (SSP1) leads to improvements in both air quality and climate, whereas SSP3 (regional rivalry) is not compatible with achieving air quality and climate goals, and the conventional fuels (SSP5) pathway improves air quality at the expense of climate (Reis et al., 2018). Strong climate and air pollutant mitigation measures in SSP1 were shown to reduce global annual mean surface $O_3$ concentrations by more than 3.5 ppb, whereas for SSP3 $O_3$ concentrations over Asia were predicted to increase by 6 ppb (Turnock et al., 2019). These studies highlighted the potential large regional variability in the response of air pollutants to the different assumptions in the future pathways and also the need for a full model assessment using the current generation of Earth system models (ESMs) that take into account both changes in emissions and climate.

In this study, we use results from experiments conducted as part of CMIP6 to make a first assessment of historical and future changes in air pollutants. First, we assess the performance of CMIP6 models in simulating present-day air pollutants by conducting an evaluation against observations of $O_3$ and $PM_{2.5}$. Regional changes in surface $O_3$ and $PM_{2.5}$ are computed over the historical period (1850–2014) to provide context with future changes. We are then able to show future projections of air pollutants over different world regions under different shared socio-economic pathways used in the CMIP6 experiments. Finally, a comparison is made of individual CMIP6 models for a single future scenario (ssp370) to identify potential reasons for model discrepancies.

## 2 Methods

### 2.1 Air pollutant emissions

A new set of historical and future anthropogenic air pollutant emissions have been developed and used as part of CMIP6. The historical anthropogenic emissions are from the Community Emissions Data System (CEDS), and a new dataset was developed for biomass-burning emissions, both of which provide information on emissions from 1750 to 2014 (van Marle et al., 2017; Hoesly et al., 2018). The SSPs used in future CMIP6 experiments represent an update from the RCPs used in CMIP5 as they combine pathways of socio-economic development with targets to achieve a certain level of climate mitigation (O'Neill et al., 2014; van Vuuren et al., 2014; Riahi et al., 2017). The SSPs are divided into the following five different pathways depending on their social, economic and environmental development: SSP1 – sustainability, SSP2 – middle of the road, SSP3 – regional rivalry, SSP4 – inequality, SSP5 – fossil fuel development. An assumption about the degree of air pollution control (strong, medium or weak) is included on top of the baseline pathway, with stricter air pollution controls assumed to be tied to economic development (Rao et al., 2016). Weak air pollution controls occur in SSP3 and SSP4, with medium controls in SSP2 and strong air pollution controls in SSP1 and SSP5 (Gidden et al., 2019). A particular climate mitigation target, in terms of an anthropogenic radiative forcing by 2100, and the range of emission mitigation measures associated with achieving it are included in addition to the existing policy measures within each baseline SSP scenario. Climate mitigation targets vary from a weak-mitigation scenario with an anthropogenic radiative forcing of $8.5\,W\,m^{-2}$ by 2100, comparable with a 5 °C temperature change (Riahi et al., 2017), to a strong-mitigation scenario with a radiative forcing of $1.9\,W\,m^{-2}$ by 2100, in accordance with the Paris Agreement for keeping temperatures below 2 °C (United Nations, 2016). Some climate mitigation targets are comparable with those of the RCPs used in CMIP5 (2.6, 4.5 and 6.0), whilst others are new; e.g. ssp534-over is included as a delayed mitigation scenario. A

scenario specific to the Aerosol and Chemistry Model Intercomparison Project (AerChemMIP), ssp370-lowNTCF, is also included to study the impact of mitigation measures to specifically control SLCFs on top of ssp370. Future biomass-burning emissions vary in each scenario, depending on the particular land-use assumptions (Rao et al., 2017). Whilst future anthropogenic and biomass-burning emissions are prescribed in each CMIP6 model from the same dataset, other natural emissions, e.g. dust, biogenic volatile organic compounds (BVOCs) etc., will be different and depend on the individual model configuration.

Figure 1 shows the future changes in global total (anthropogenic and biomass) emissions of the major air pollutant precursors across all of the CMIP6 scenarios, provided as input to the CMIP6 models. The overlying feature is that global air pollutant emissions are predicted to reduce across the majority of scenarios by 2100. The exception to this is that global and regional emissions increase or remain at present-day levels for ssp370 (Figs. 1 and 2). Some air pollutant emissions increase in the near term in other scenarios, e.g. nitrogen oxides ($NO_x$) in ssp585 (by up to 15 %), but by 2100 these have been reduced. Future $CH_4$ abundances show the largest diversity amongst the SSPs. Large increases in global $CH_4$ abundances of more than 50 % are predicted for the fossil-fuel-dominated pathways of ssp370 and ssp585, whereas large reductions of $\sim 50$ % are predicted to occur in the strong-mitigation scenarios of SSP1.

For $SO_2$ large reductions of more than 50 % are shown for most scenarios and across most regions (Fig. 2), apart from Africa and Asia in ssp370. Near-term (2050) increases in $SO_2$ occur over South Asia and other developing regions, which are then reduced in the latter half of the 21st century. Over Europe and North America, consistent decreases are predicted across all scenarios. The other major aerosol emissions, OC and BC, show similar reductions to $SO_2$ across all scenarios and regions. For all aerosol and aerosol precursors, a reduction of 80 %–100 % (relative to 2015) in regional emissions is predicted by 2100 in the strong-mitigation scenarios. Changes in the emissions of the $O_3$ precursors – $NO_x$, CO and non-methane volatile organic compounds (NMVOCs) – show a similar increase across most regions for ssp370 but a general decrease in other scenarios. The change in these emissions is particularly diverse across all the scenarios in South Asia, with large relative increases in ssp370 (of up to 50 %) in contrast to the large decreases in ssp126 (up to 40 %). Across East Asia there is a 20 % increase in $NO_x$ emissions for ssp370 in 2050 but a long-term reduction across all scenarios.

### 2.2 CMIP6 simulations

Surface concentrations of $O_3$ and $PM_{2.5}$ have been obtained from all the CMIP6 models that made appropriate data available to the Earth System Grid Federation (ESGF) at the time of writing. To study changes in surface air pollutants over the industrial period, data have been obtained from the coupled historical simulations (Eyring et al., 2016) over the period 1850 to 2014 from all of the available ensemble members of each available CMIP6 model. For each model, a mean is taken using all available ensemble members prior to the calculation of the multi-model mean. For model evaluation purposes, 10 years of data from historical simulations have been used over the period that is relevant to the particular observational dataset (2000–2010 for ground-based $PM_{2.5}$, 2004–2014 for $PM_{2.5}$ reanalysis product and 2005–2014 for ground-based $O_3$). To investigate future changes in air pollutants, all available data have been obtained over the period 2015 to 2100 for each of the different future coupled atmosphere–ocean model experiments, conducted as part of ScenarioMIP (O'Neill et al., 2016). CMIP6 model data have also been obtained for the AerChemMIP specific ssp370-lowNTCF scenario, which was only required to be conducted over the period 2015–2055 (Collins et al., 2017).

Concentrations of both pollutants at the surface have been obtained by extracting the lowest vertical level of the full 3D field output on the horizontal and vertical grid of each model (the "AERmon" CMIP6 table ID). For $O_3$, this is supplied as a separate diagnostic which can be used directly. However, models contributing to CMIP6 will not all directly output $PM_{2.5}$, and the calculation of $PM_{2.5}$ will not be consistent across individual models due to the different treatment of aerosols and their components. For example only a few CMIP6 models include the simulation of ammonium nitrate in their aerosol scheme (currently, only GISS-E2-1-G and GFDL-ESM4 have provided nitrate mass mixing ratios on the ESGF database). Therefore, to use a consistent definition across all models, we calculated $PM_{2.5}$ offline. In this study, surface $PM_{2.5}$ is defined as the sum of the individual dry aerosol mass mixing ratios of black carbon (BC), total organic aerosol (OA – both primary and secondary sources), sulphate ($SO_4$), sea salt (SS) and dust (DU) from the lowest model level extracted from the full 3D model fields. All BC, OA and $SO_4$ aerosol mass is assumed to be present in the fine size fraction ($< 2.5\,\mu m$), whereas a factor of 0.25 for SS and 0.1 for DU has been used to calculate the approximate contribution from these components to the fine aerosol size fraction (Eq. 1).

$$PM_{2.5} = BC + OA + SO_4 + (0.25 \times SS) + (0.1 \times DU) \quad (1)$$

The factors used to calculate the contribution of SS and DU concentrations to the $PM_{2.5}$ size fraction are likely to depend on the individual aerosol scheme and the simulated aerosol size distribution within a particular model. The calculation of an approximate $PM_{2.5}$ concentration using Eq. (1) is therefore likely to introduce some errors, but it does provide an estimate that is consistent across models and also with that previously used in CMIP5 and ACCMIP (Fiore et al., 2012; Silva et al., 2013, 2017). For the CNRM-ESM2-1 model, anomalously large concentrations were obtained from the sea

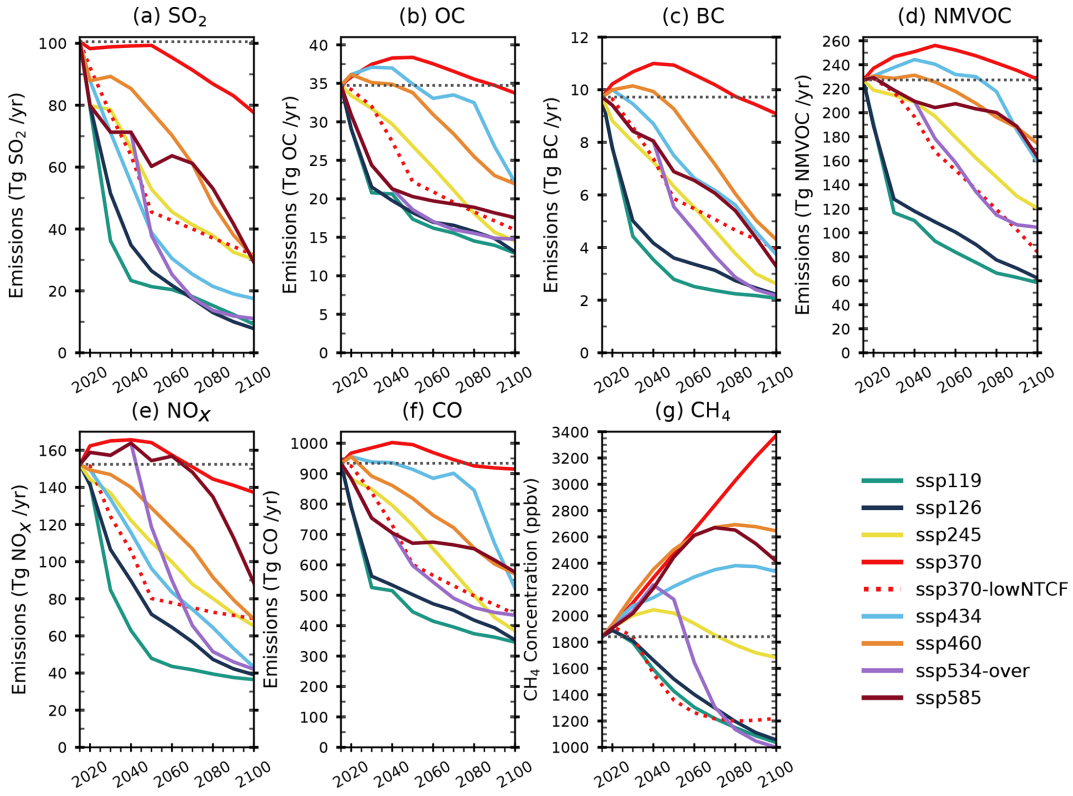


**Figure 1.** Changes in annual total (anthropogenic and biomass) global air pollutant emissions (relative to 2015) of sulphur dioxide ($SO_2$), organic carbon (OC), black carbon (BC), non-methane volatile organic compounds (NMVOCs), nitrogen oxides ($NO_x$), carbon monoxide (CO) and global methane ($CH_4$) abundances in the future CMIP6 scenarios used as input to CMIP6 models. The dashed black line represents the 2015 value. Global $CH_4$ abundances are not reduced in the AerChemMIP ssp370-lowNTCF simulations used here.

salt mass mixing ratios. Sensitivity tests with this model suggested that a much smaller factor of 0.01 was more appropriate to use for SS, which takes into account the non-dry nature of the sea salt aerosols and the large possible size range, up to 20 µm in diameter, of sea salt particles within the CNRM-ESM2-1 model (Pierre Nabat, personal communication, 27 November 2019).

Details of the data used in this study from different CMIP6 models, in both the historical and future scenarios, are presented in Table 1. For the historical period, data were available from 6 different CMIP6 models for $O_3$ and 11 models for $PM_{2.5}$. The future scenario with the most data available was ssp370, with 6 models supplying data for $O_3$ and 10 models for $PM_{2.5}$. For the other Tier 1 CMIP6 scenarios (ssp126, ssp245 and ssp585), data were only available for four models for $O_3$ and seven for $PM_{2.5}$ (all components). It was decided to focus the analysis on ssp370 and other Tier 1 scenarios due to the limited availability of model data for Tier 2 scenarios (ssp119, ssp434, ssp460 and ssp534-over). The results from an $O_3$ parameterisation (Turnock et al., 2018, 2019), referred to in this study as HTAP_param, have also been included in the analysis of surface $O_3$ from CMIP6 models for both the historical and future scenarios. The HTAP_param was previously developed based upon the source–receptor relationships of $O_3$ derived from perturbation experiments of regional precursor emissions and global $CH_4$ abundances (Wild et al., 2012; Turnock et al., 2018). The HTAP_param applies the fractional change in global $CH_4$ abundance and regional-emission precursors ($NO_x$, CO and NMVOCs) for a particular scenario to the ozone response from each individual model used in the parameterisation. The total $O_3$ response is obtained by summing up the response from each of the individual models to all precursor changes across all source regions. The surface $O_3$ response previously calculated from the HTAP_param in both the historical and future CMIP6 scenarios is compared to that from the CMIP6 models (Turnock et al., 2019). The $O_3$ parameterisation does not take into account the effects of climate change on surface $O_3$ concentrations and therefore provides an estimate of the emission-only-driven changes to surface $O_3$, which we compare to the climate and Earth system models.

### 2.3 Surface observations

Present-day surface $O_3$ and $PM_{2.5}$ simulated by all of the CMIP6 models are evaluated against surface observations to

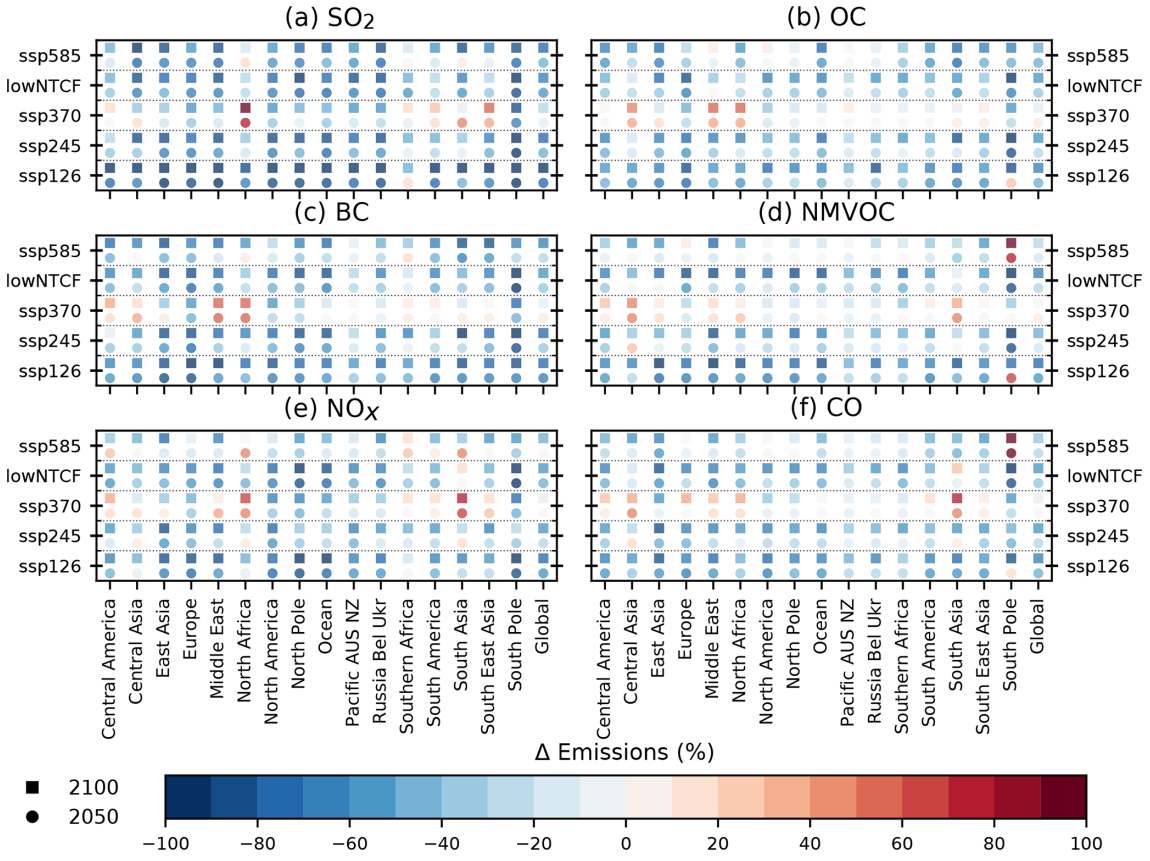


**Figure 2.** Percentage change in 2050 (circles) and 2100 (squares), relative to 2015, for annual mean total (anthropogenic and biomass) air pollutant emissions of **(a)** $SO_2$, **(b)** OC, **(c)** BC, **(d)** NMVOCs, **(e)** $NO_x$ and **(f)** CO across different world regions in the four Tier 1 future CMIP6 scenarios and the ssp370-lowNTCF scenario (identified as lowNTCF). Regions are defined in Fig. S1 in the Supplement.

ascertain model biases and inter-model discrepancies. Surface $O_3$ observations are obtained from the database of the Tropospheric Ozone Assessment Report (TOAR; Schultz et al., 2017). The TOAR database provides a gridded product of surface $O_3$ observations over the period 1970 to 2015. The majority of measurement sites are located in North America and Europe, with a smaller number of other sites in East Asia, Australia, New Zealand, South America, Southern Africa, Antarctica and remote ocean locations. Here we compile a monthly mean climatology of all available $O_3$ observations over the period 2005–2014 from measurement locations that are classified as rural in the TOAR database (Schultz et al., 2017). The rural locations were selected to be representative of background (i.e. non-urban) $O_3$ concentrations and are considered to be more appropriate in evaluating the simulated values obtained at the relatively coarse horizontal resolution of the global ESMs. Simulated surface $O_3$ concentrations from the CMIP6 models are re-gridded onto the same resolution of the observational product ($2° \times 2°$) for evaluation purposes.

Surface $PM_{2.5}$ observations have been obtained from all of the locations compiled in the database of the Global Aerosol Synthesis and Science Project (GASSP; http://gassp.org.uk/data/, last access: 2 July 2020, Reddington et al., 2017) to evaluate CMIP6 models. Background, non-urban $PM_{2.5}$ data are compiled in the GASSP database from three major networks: the Interagency Monitoring of Protected Visual Environments (IMPROVE) network in North America, the European Monitoring and Evaluation Programme (EMEP), and Asia-Pacific Aerosol Database (A-PAD). Again, like for $O_3$, the networks and observations for $PM_{2.5}$ were selected to be representative of non-urban environments, which are more appropriate for the evaluation of global ESMs. With the exception of the IMPROVE network, most measurements of $PM_{2.5}$ began after the year 2000. Like for $O_3$, we compile a monthly mean climatology of $PM_{2.5}$ but now over the period of 2000 to 2010, selected because the GASSP database contained the most observations within this period. Simulated surface $PM_{2.5}$ was computed from CMIP6 models over the same time period as the observations and linearly interpolated to each measurement location. Whilst the surface observations measure total $PM_{2.5}$ mass, the computed $PM_{2.5}$ from CMIP6 models uses Eq. (1) and does not include all observable $PM_{2.5}$ aerosol components (e.g. nitrate aerosol).

**Table 1.** Number of ensemble members used for the historical- and future-scenario experiments from each model in the analysis of surface $O_3$ and $PM_{2.5}$ in this study.

| Model | Pollutant | Historical | ssp126 | ssp245 | ssp370 | ssp370-lowNTCF | ssp585 | Model references | Data citation |
|---|---|---|---|---|---|---|---|---|---|
| BCC-ESM1 | $O_3$, $PM_{2.5}$ | 3 | | | 3 | 3 | | Wu et al. (2019, 2020) | Zhang et al. (2018, 2019) |
| CESM2-WACCM | $O_3$, $PM_{2.5}$ | 3 | | | 1 | 1 | | Gettelman et al. (2019), Tilmes et al. (2019), Emmons et al. (2020) | Danabasoglu (2019a–c) |
| CNRM-ESM2-1 | $PM_{2.5}$ | 3 | | | 3 | 3 | | Michou et al. (2019), Séférian et al. (2019) | Seferian (2018, 2019), Voldoire (2019) |
| GFDL-ESM4 | $O_3$, $PM_{2.5}$ | 1 | 1 | 1 | 1 | 1 | 1 | Horowitz et al. (2020), Dunne et al. (2020) | Horowitz et al. (2018), John et al. (2018), Krasting et al. (2018) |
| HadGEM3-GC31-LL | $PM_{2.5}$ | 4 | 1 | 1 | | | 1 | Kuhlbrodt et al. (2018) | Ridley et al. (2018); Good (2019) |
| MIROC6-ES2L | $PM_{2.5}$ | 3 | 1 | 1 | 1 | | 1 | Takemura (2012), Hajima et al. (2020) | Hajima and Kawamiya (2019), Tachiiri and Kawamiya (2019) |
| MPI-ESM1.2-HAM | $PM_{2.5}$ | 1 | | | 1 | 1 | | Tegen et al. (2019) | Neubauer et al. (2019) |
| MRI-ESM2-0 | $O_3$, | 5 | 1 | 1 | 3 | 1 | 1 | Yukimoto et al. (2019d), Oshima et al. (2020) | Yukimoto et al. (2019a–c) |
| | $PM_{2.5}$ | 5 | 1 | 1 | 3 | 1 | 1 | | |
| GISS-E2-1-G | $O_3$, | 5 | 1 | 5 | 1 | | 1 | Bauer et al. (2020) | NASA Goddard Institute For Space Studies (NASA/GISS; 2018) |
| | $PM_{2.5}$ | 4 | 1 | 5 | 1 | | 1 | | |
| NorESM2-LM | $PM_{2.5}$ | 1 | 3 | 3 | 3 | 3 | 3 | Karset et al. (2018), Kirkevåg et al. (2018) | Norwegian Climate Center (NCC; 2018) |
| UKESM1-0-LL | $O_3$, $PM_{2.5}$ | 5 | 5 | 5 | 5 | 3 | 5 | Sellar et al. (2019) | Good et al. (2019); Tang et al. (2019) |
| Total number of models | $O_3$ | 6 | 4 | 4 | 6 | 5 | 4 | | |
| | $PM_{2.5}$ | 11 | 7 | 7 | 10 | 8 | 7 | | |

Therefore, it is anticipated that the CMIP6 models will underrepresent the $PM_{2.5}$ observations in this comparison.

To address the anticipated disparity between the observed ground-based $PM_{2.5}$ and the approximate $PM_{2.5}$ from CMIP6 models, a further comparison has been made between the CMIP6 models and the Modern-Era Retrospective Analysis for Research and Applications, version 2 (MERRA-2), aerosol reanalysis product (Buchard et al., 2017; Randles et al., 2017). The MERRA-2 aerosol product assimilates observations of aerosol optical depth (AOD) from ground-based and satellite remote-sensing platforms into model simulations that use the GEOS-5 atmospheric model coupled to the GOCART aerosol module. The data assimilation used in MERRA-2 generally improves comparisons of $PM_{2.5}$ with observations, but there are still overestimations due to dust and sea salt and underestimations over East Asia (Buchard et al., 2017; Provençal et al., 2017). Separate mass mixing ratios for BC, OA, $SO_4$, SS and DU aerosol components are provided from MERRA-2, which are then combined using the formula in Eq. (1) to make an approximate $PM_{2.5}$. Monthly mean approximate $PM_{2.5}$ concentrations are then computed over the period 2005–2014 from the MERRA-2 reanalysis product to provide a more direct comparison and enhanced spatial coverage against the approximate $PM_{2.5}$ concentrations calculated from the CMIP6 models calculated over the same time period.

## 3 Present-day model evaluation of air pollutants

### 3.1 Surface ozone

The six CMIP6 models with data available for the historical experiments are evaluated against surface $O_3$ observations from the TOAR database over the period 2005–2014. A long-term evaluation of surface $O_3$ concentrations from CMIP6 models using observations compiled over the 20th century is presented separately in Griffiths et al. (2020). Figure 3 shows the annual and seasonal multi-model mean in surface $O_3$ over the period 2005–2014 and the SD across the six CMIP6 models. The annual and seasonal mean surface $O_3$ concentrations and evaluation against observations for individual CMIP6 models are shown in Figs. S2–S7. Higher surface $O_3$ concentrations are simulated in the Northern Hemisphere summer (June, July, August – JJA) when $O_3$ formation is enhanced by increased photolytic activity and levels of oxidants as well as larger biogenic emissions. The hemispheric difference in surface $O_3$ is smaller in December, January and February (DJF) when $O_3$ production is less in the Northern Hemisphere but higher in the Southern Hemisphere. However, model diversity is larger in DJF (Fig. 3e) due to individual models simulating different seasonal cycles of $O_3$, particularly UKESM1-0-LL which has the most pronounced seasonal cycle of all 6 models (Fig. S2).

The multi-model mean of CMIP6 models overestimates surface $O_3$ concentrations by up to 16 ppb annually and in

both seasons when compared to observations from the TOAR database, although they do capture the broad hemispheric gradient in $O_3$ concentrations (Fig. 3c, f and i). The model observational comparison of CMIP6 models to the TOAR observations is consistent across all models and with the previous evaluation of ACCMIP models (Young et al., 2018). This indicates a common source of error within models, for example uncertainties in emission inventories, deposition processes or vertical mixing (Wild et al., 2020). In addition, the coarse resolution of the ESMs could lead to an overproduction of $O_3$ across polluted regions, with finer resolutions exhibiting improvements in the simulation of surface $O_3$ (Wild and Prather, 2006; Neal et al., 2017). Smaller model biases exist in DJF ($< 5$ ppb) than in JJA (5–15 ppb), mostly attributed to the strong seasonal cycle simulated by UKESM1-0-LL. In contrast to other models (Figs. S2–S7), UKESM1-0-LL underpredicts surface $O_3$ in DJF over most continental Northern Hemisphere locations, potentially indicating there is excessive $NO_x$ titration of $O_3$ in this model, which is also shown by the large sensitivity of $O_3$ formation to $NO_x$ concentrations over the historical period (Fig. S17).

The observed annual cycle in surface $O_3$ averaged across measurement locations within different regions is compared to that simulated by CMIP6 models (Fig. 4). Across most regions, the mean annual cycle from CMIP6 models compares relatively well to that observed. The overprediction of surface $O_3$ values in JJA is evident across most regions, as are the large concentrations in BCC-ESM1 and GISS-E2-1-G and the strong seasonal cycle in UKESM1-0-LL across Northern Hemisphere continental regions. Additionally, the timing of peak $O_3$ over continental Northern Hemisphere locations occurs earlier in the observations (springtime) than in the CMIP6 models (spring and summer), which is consistent with that from ACCMIP models (Young et al., 2018). At oceanic observation locations, surface $O_3$ is overestimated in CMIP6 models by up to 20 ppb across all seasons, indicating that the $O_3$ deposition rate could be underestimated here (Clifton et al., 2020). There is also a large overestimation ($\sim 20$ ppb) in all models at the one observation location in South East Asia, potentially due to difficulty in simulating $O_3$ in the maritime continental boundary layer using lower-resolution global ESMs. In contrast to this, CMIP6 models, particularly UKESM1-0-LL and GISS-E2-1-G, tend to underpredict the observed surface $O_3$ concentrations at locations in the South Pole region in JJA by $\sim 5$ ppb. This could be due to lack of long-range transport of $O_3$ to these sites, inaccuracies in Southern Hemisphere precursor emissions or because of the difficulty in simulating $O_3$ concentrations at the appropriate elevation of measurement sites located on the Antarctic Ice Sheet.

### 3.2 Surface $PM_{2.5}$

#### 3.2.1 Ground-based observations

A similar comparison is made for annual and seasonal mean surface $PM_{2.5}$ concentrations from CMIP6 models against ground-based surface observations (Fig. 5). The annual and seasonal multi-model mean from CMIP6 models shows that elevated $PM_{2.5}$ concentrations ($> 50\,\mu g\,m^{-3}$) occur close to the large dust emission source regions of the Sahara and Middle East in both DJF and JJA over 2000–2010. These natural source regions are also one of the largest areas of diversity in $PM_{2.5}$ concentrations (up to $20\,\mu g\,m^{-3}$) between the different CMIP6 models (Fig. 5b, e, h and Fig. S8). High concentrations of $PM_{2.5}$ ($> 40\,\mu g\,m^{-3}$) are also simulated over the large anthropogenic source regions of South and East Asia, particularly in DJF, when there is enhanced variability across CMIP6 models due to the different contribution from anthropogenic $PM_{2.5}$ components (Figs. S9–S11). The diversity in the CMIP6 models is particularly evident in the organic-aerosol concentrations across Asia, with higher present-day values simulated by CESM2-WACCM and UKESM1-0-LL and lower values in CNRM-ESM2-1 and MIROC-ES2L (Fig. S11). Lower $PM_{2.5}$ concentrations ($< 10\,\mu g\,m^{-3}$) are predicted across both North America and Europe, with more agreement between CMIP6 models. Across the biomass-burning regions of South America and Southern Africa, $PM_{2.5}$ concentrations are elevated in JJA, with larger diversity in the CMIP6 models due to the differing contributions of the BC and OA components, particularly shown in NorESM2-LM, GISS-E2-1-G and GFDL-ESM4 (Figs. S10 and S11). Relatively consistent $PM_{2.5}$ concentrations of $< 10\,\mu g\,m^{-3}$, with small model diversity ($< 5\,\mu g\,m^{-3}$), are shown across oceanic regions, mainly from emissions of sea salt (Fig. S12). Apart from the natural sources of aerosol, which are subject to meteorological variability, the CMIP6 models are relatively consistent when simulating $PM_{2.5}$ concentrations across most regions.

Compared to the ground-based observations from the GASSP database, the CMIP6 multi-model mean underpredicts the observed $PM_{2.5}$ values by up to $10\,\mu g\,m^{-3}$ in both seasons, with a slightly larger underestimation in DJF than JJA. As discussed in Sect. 2.3, an underestimation was anticipated from comparing approximate $PM_{2.5}$ concentrations derived from CMIP6 models to observed values. Nevertheless, the evaluation highlights that fine particulate matter ($PM_{2.5}$) is generally underrepresented in the CMIP6 models across North America, Europe and parts of Asia for which observations are available, a similar result to other studies evaluating global and regional models (Tsigaridis et al., 2014; Pan et al., 2015; Glotfelty et al., 2017; Solazzo et al., 2017; Im et al., 2018). Numerous reasons potentially exist for the model observation discrepancy shown here and in other studies, including uncertainties in emission inventories (e.g. local dust sources), errors in the wet and dry deposition schemes,

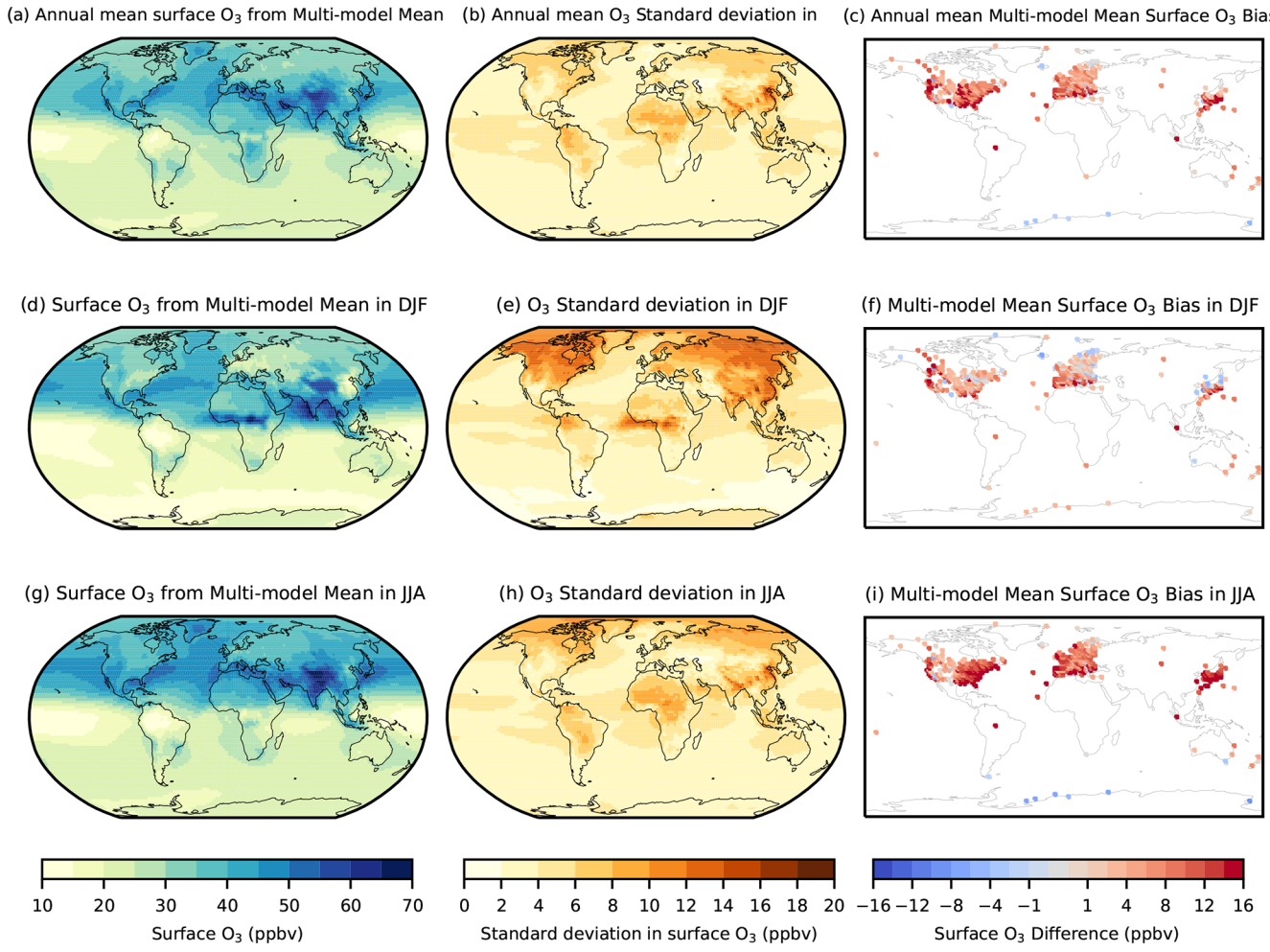


**Figure 3.** Multi-model (six CMIP6 models) annual and seasonal mean surface $O_3$ concentrations over the 2005–2014 period in **(a)** annual mean; **(d)** December, January and February (DJF); and **(g)** June, July and August (JJA). The SD of the multi-model mean in **(b)** annual mean, **(e)** DJF and **(h)** JJA. The difference between the multi-model mean and TOAR observations in **(c)** annual mean, **(f)** DJF and **(i)** JJA (colour bar saturates).

the absence or underrepresentation of aerosol formation processes (e.g. secondary organic aerosols), and the coarse resolution of global models leading to errors in emissions and simulated meteorology. Understanding the causes of model observational discrepancies is an area of active research and should be explored in further research, for example in a global multi-model sensitivity study that examines model uncertainties.

The simulated regional mean annual cycle in surface $PM_{2.5}$ from different CMIP6 models against observations is shown in Fig. 6. The low model bias in $PM_{2.5}$ concentrations is highlighted across all regions, except for the ocean region, where there is a relatively large diversity in model simulations, particularly MIROC-ES2L and NorESM2-LM, at these observation locations. Across North America, the region with the most observations, the annual cycle is simulated relatively well, with a peak in concentrations in JJA and a lower model bias, although a larger model bias (factor of $\sim 1.5$ to 2) occurs in winter and spring. Across Europe, there is a larger underestimation of observed $PM_{2.5}$ concentrations by CMIP6 models in DJF (factor $> 2$) than JJA. Nitrate aerosols are observed and modelled (from two CMIP6 models in Fig. S13) to contribute between 1 and 5 $\mu g\,m^{-3}$ of the total aerosol mass over Europe (Fagerli and Aas, 2008; Pozzer et al., 2012), explaining part, but not all, of the model observational discrepancy here. Additionally, in Fig. 6 the CMIP6 models also underestimate the MERRA-2 reanalysis product (which does not include nitrate aerosols), indicating that other aerosol sources and processes are underrepresented across Europe and other regions in the models. The limited number of observations across other regions makes it difficult to infer particular model observational biases. However, over Asia CMIP6 $PM_{2.5}$ concentrations tend to be within a factor of 2 of the observations and represent the seasonal

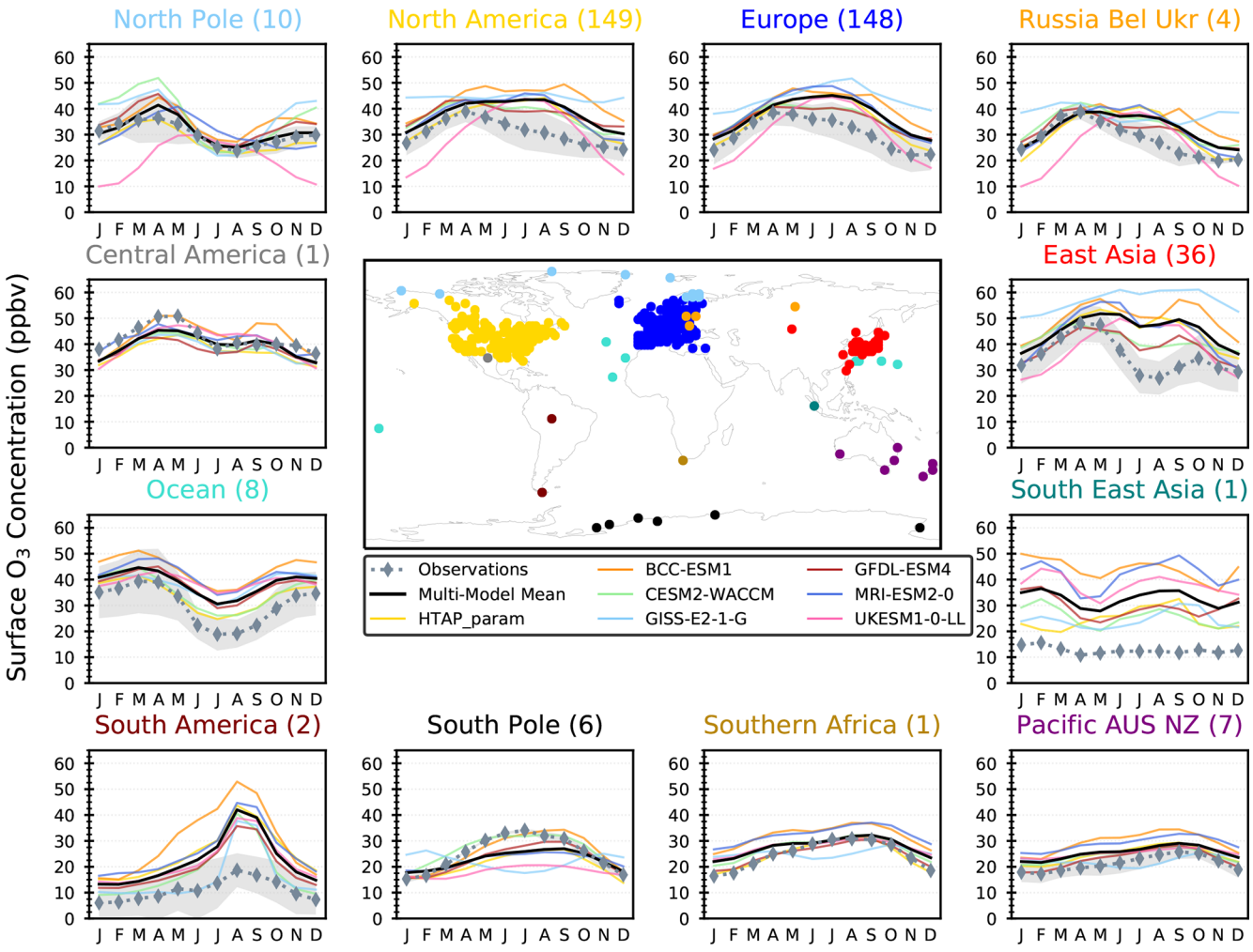


**Figure 4.** Individual and multi-model (six CMIP6 models and HTAP_param) monthly mean surface $O_3$ concentrations across different world regions compared with the regional monthly values from all the TOAR observations within the region for the period 2005–2014. The number of observations within a region is shown in parentheses. The shading shows variability in observations across all sites within the region.

cycle relatively well at these locations. Over Asia, larger $PM_{2.5}$ concentrations are simulated in the CMIP6 models CESM2-WACCM, HadGEM3-GC31-LL and UKESM1-0-LL, mainly due to the larger OA component (Fig. S11). Across South Asia, concentrations are relatively well simulated in JJA, but a larger discrepancy ($15\,\mu g\,m^{-3}$) exists in DJF between the model and observations.

### 3.2.2 MERRA reanalysis product

An additional comparison of surface $PM_{2.5}$ concentrations from the MERRA-2 aerosol reanalysis product is made with that simulated by the CMIP6 models to improve the spatial coverage and provide a more consistent evaluation of the approximate $PM_{2.5}$ concentrations. Fig. 7 shows the same comparison as in Fig. 5 but now using the approximate $PM_{2.5}$ obtained from the MERRA-2 reanalysis product over the period 2005–2014. In comparison to MERRA-2, the CMIP6 models are shown to underpredict $PM_{2.5}$ concentrations across North America, Europe and Eurasia but by a smaller amount in comparison to ground-based observations. A similar seasonal-cycle comparison is shown for Europe and North America (regions with most ground-based observations) in both Figs. 6 and 8, providing confidence that the underestimation of $PM_{2.5}$ by CMIP6 models is robust over these regions. Across all other regions, the MERRA-2 reanalysis product provides much greater spatial coverage for each region, and therefore the features shown in the site-level comparison (Fig. 6) will not necessarily apply here. A large overestimation of the MERRA-2 reanalysis product by the CMIP6 multi-model mean is shown across East and South Asia. Figure 8 shows that on a regional mean basis, most CMIP6 models are within the spread of the MERRA-2 concentrations for East Asia, although MERRA-2 was previously shown to underestimate $PM_{2.5}$ concentrations across East Asia (Buchard et al., 2017; Provençal et al., 2017) and

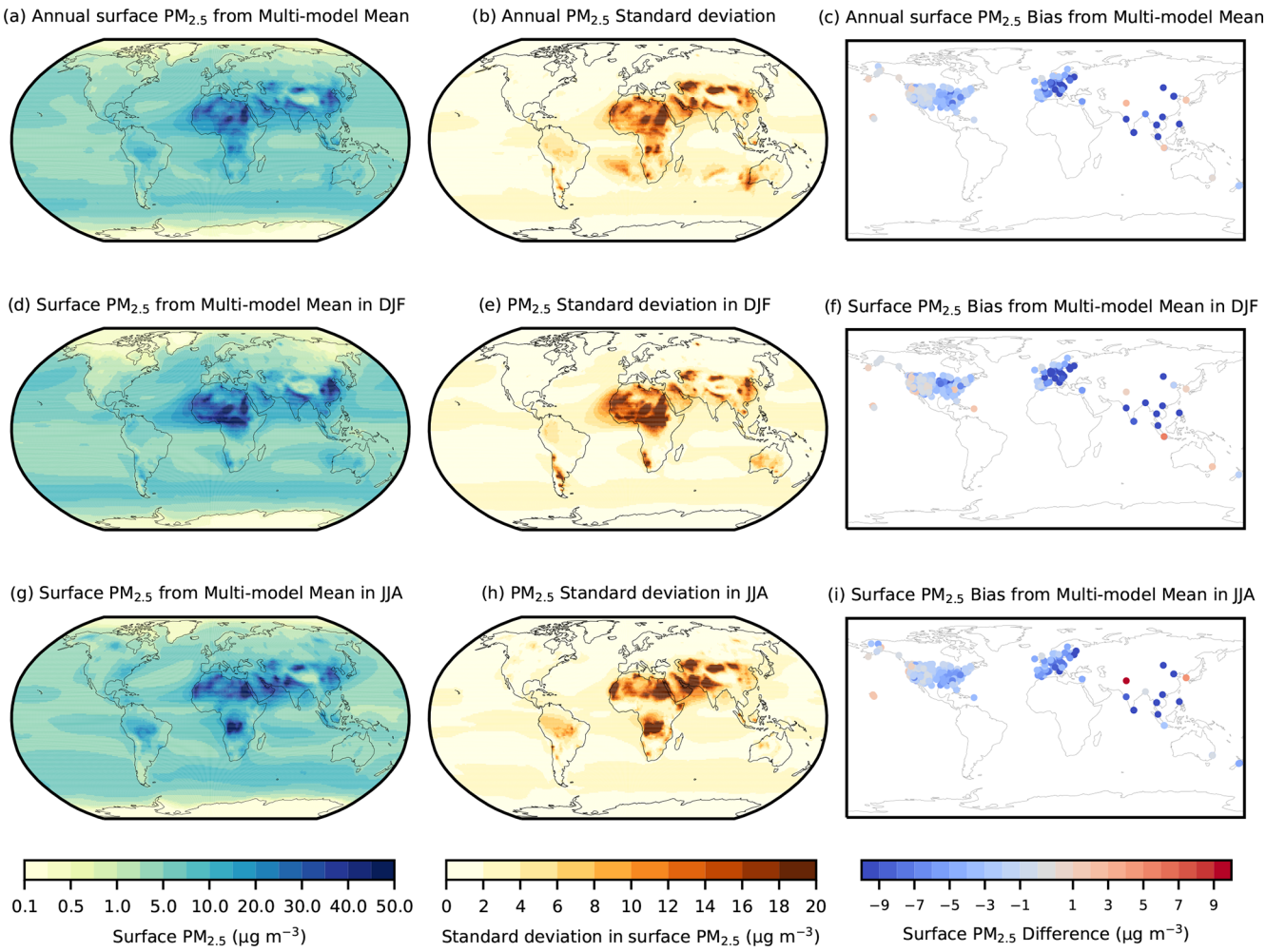


**Figure 5.** Multi-model (11 CMIP6 models) annual and seasonal mean surface $PM_{2.5}$ concentrations over the 2000–2010 period in **(a)** annual mean; **(d)** December, January and February (DJF); and **(g)** June, July and August (JJA). The SD of the multi-model mean in **(b)** annual mean, **(e)** DJF and **(h)** JJA. The difference between the multi-model mean and $PM_{2.5}$ observations in **(c)** annual mean, **(f)** DJF and **(i)** JJA (colour bar saturates).

also in Fig. 6. CESM2-WACCM and MRI-ESM2-0 are the exceptions to this, with distinctly higher $PM_{2.5}$ concentrations over East Asia, potentially due to larger OA concentrations and more dust aerosols within the western side of this region (Figs. S8 and S11). Across the South Asian region, CMIP6 models consistently overestimate MERRA-2 by more than $10\,\mu g\,m^{-3}$ in certain months. UKESM1-0-LL, MRI-ESM2-0 and CESM2-WACCM simulate particularly high monthly $PM_{2.5}$ concentrations of 20–40 $\mu g\,m^{-3}$ over South Asia due to large contributions from $SO_4$, dust and OA. Across North Africa there is considerable variability in $PM_{2.5}$ within this region as CMIP6 models both under- and overestimate the MERRA-2 $PM_{2.5}$ concentrations, although this results in a relatively good regional mean representation (Figs. 7 and 8). The annual mean cycle in MERRA-2 $PM_{2.5}$ concentrations across South America is well represented by the CMIP6 models, although the peak in the biomass-burning season is underestimated by 5–10 $\mu g\,m^{-3}$ in some models. A more pronounced annual cycle is exhibited by UKESM1-0-LL across Southern Africa due to the larger contributions from the OA fraction (Fig. S11), potentially from enhanced biogenic emissions that result in secondary OA formation (SOA). Across oceanic locations all of the CMIP6 models underestimate the MERRA-2 $PM_{2.5}$ concentrations by $5\,\mu g\,m^{-3}$, although MERRA-2 was previously shown to overestimate sea salt concentrations (Buchard et al., 2017; Provençal et al., 2017), accounting for some of this discrepancy. Overall, comparisons of CMIP6 models with the MERRA-2 reanalysis product show biases across Europe and North America that are consistent with the comparison to ground-based observations. Additionally, similar comparisons are shown in annual mean cycles across other regions, for which appropriate ground-based data are lacking.

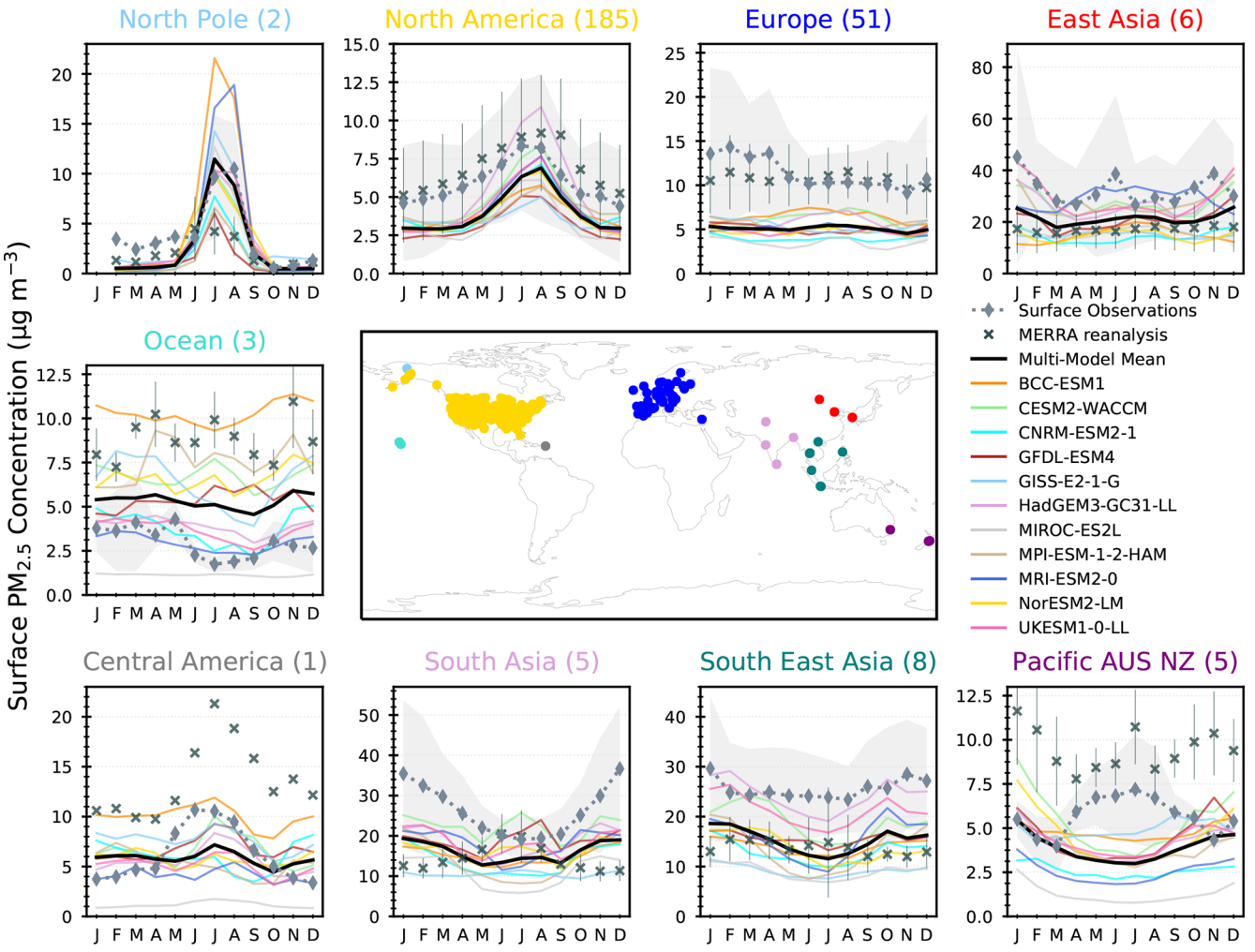


**Figure 6.** Individual and multi-model (11 CMIP6 models) monthly mean surface $PM_{2.5}$ concentrations across different world regions compared with the regional monthly values from all the $PM_{2.5}$ observations (◇) and the MERRA-2 reanalysis product (×) within the region for the period 2000–2010. The number of observations within the region is shown in parentheses. The shading and errors bars show variability in observations and the reanalysis product across all sites within the region.

## 4 Air pollutants from the pre-industrial period to present day

### 4.1 Surface ozone

The simulated changes in surface $O_3$ across six CMIP6 models and the HTAP_param are shown in Fig. 9 and Figs. S14–S15 over the historical period of 1850 to 2014. The CMIP6 multi-model mean shows that global annual mean surface $O_3$ has increased by $11.7 \pm 2.3$ ppb since 1850 ($\pm 1$ SD), although the change could be as large as 14 ppb (from BCC-ESM1) or as little as 7 ppb (from UKESM1-0-LL). Globally and over most regions there has been a larger historical increase in surface $O_3$ in JJA than in DJF (Fig. S16). The 1850 to 2000 multi-model annual mean change in surface $O_3$ from the CMIP6 models of 10.6 ppb is in good agreement with the $10 \pm 1.6$ ppb simulated by the CMIP5 models used in ACCMIP (Young et al., 2013). An evaluation of the long-term changes in surface $O_3$ over the historical period simulated by the CMIP6 models at specific measurement locations is presented separately in the tropospheric $O_3$ CMIP6 companion paper of Griffiths et al. (2020). This shows that CMIP6 models can reasonably represent long-term changes in surface ozone since the 1960s, providing a degree of confidence in the future projections of changes in the CMIP6 scenarios. However, long-term changes in simulated surface $O_3$ from the previous generation of global coupled chemistry–climate models (used in CMIP5) were found to underestimate the observed trend at Northern Hemisphere monitoring locations (Parrish et al., 2014). Further comparisons of historical surface $O_3$ simulated by CMIP6 models with long-term historical observations are outside the scope of the current work but will be the subject of future research.

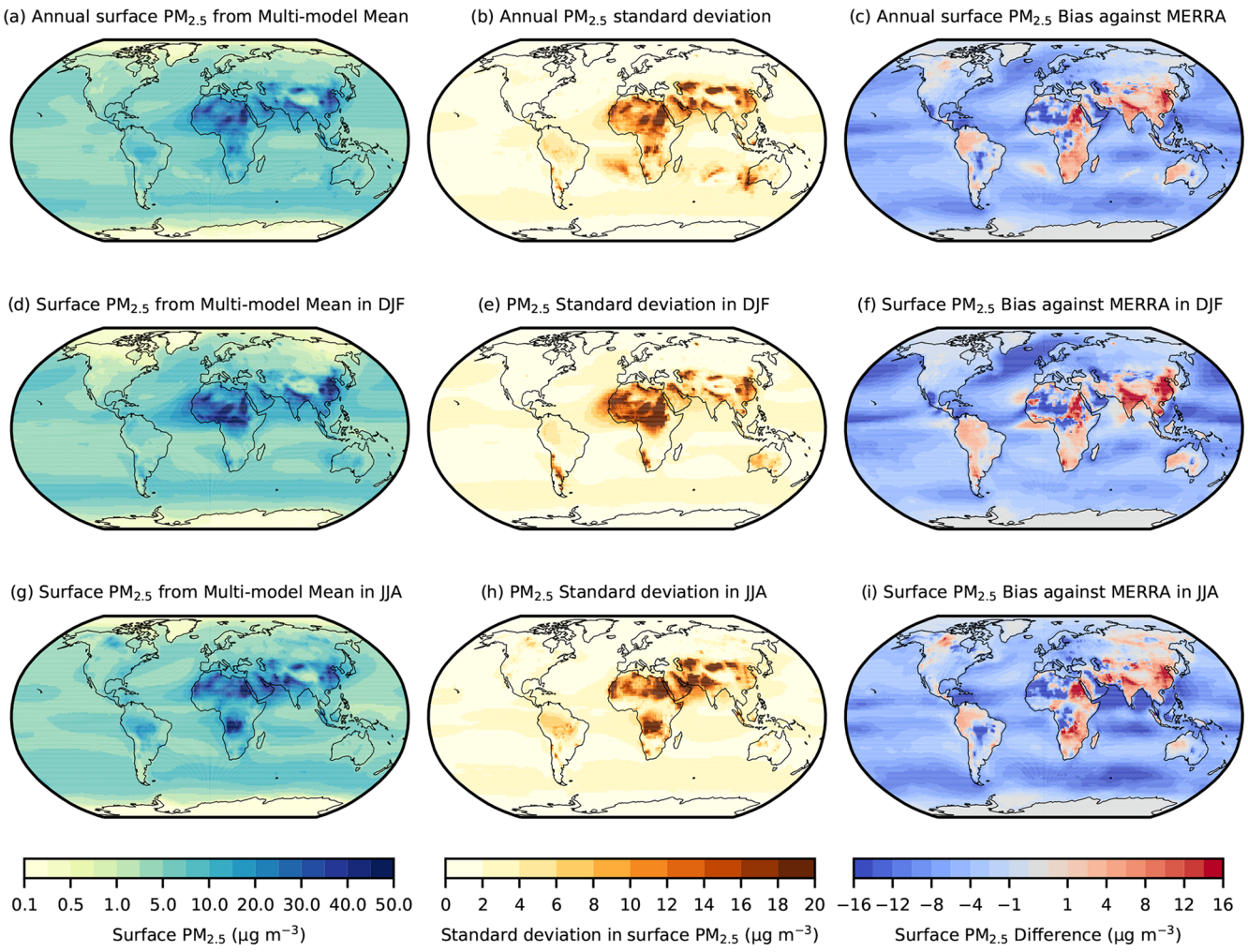


**Figure 7.** Multi-model (11 CMIP6 models) annual and seasonal mean surface $PM_{2.5}$ concentrations over the 2005–2014 period in **(a)** annual mean; **(d)** December, January and February (DJF); and **(g)** June, July and August (JJA). The SD of the multi-model mean in **(b)** annual mean, **(e)** DJF and **(h)** JJA. The difference between the multi-model mean and MERRA-2 reanalysis for **(c)** annual mean, **(f)** DJF and **(i)** JJA.

A large diversity in the simulated historical changes is shown across the different regions analysed here, with UKESM1-0-LL tending to simulate the smallest historical change and GISS-E2-1-G or BCC-ESM1 the largest. The large diversity across CMIP6 models in the surface $O_3$ response over the historical period can be attributed to the different magnitude of simulated $O_3$ concentrations in the 1850 period (Fig. S14) and the rate of change in regional mean $O_3$ concentrations (Fig. S15), which is related to the different chemical sensitivity of $O_3$ formation in each model to changing $NO_x$ concentrations (Fig. S17). Larger differences between CMIP6 models are shown in the DJF mean historical changes over Northern Hemisphere regions than what occurred in JJA (Fig. S16), reflecting the differences shown in the model evaluation (Fig. 4) and the strong seasonality of the changes. Even though the historical surface $O_3$ response is small in UKESM1-0-LL, it is shown to have larger tropospheric changes in $O_3$ over the historical period compared to other CMIP6 models (Griffiths et al., 2020).

South Asia is the region with the largest diversity in simulated historical changes in surface $O_3$, between 16 and 40 ppb, with a larger range in DJF (10–40 ppb) than in JJA (19–36 ppb). The large diversity in CMIP6 models is attributed to the large differences in simulated $NO_x$ concentrations and hence chemical sensitivities of $O_3$ formation occurring across South Asia over the historical period (Fig. S17). In addition, the large historical change in $PM_{2.5}$ over this region (Fig. S18) could alter the heterogeneous loss rate of radicals to aerosols and therefore also affect $O_3$ formation. Surface $O_3$ is simulated to have increased by between 10 and 30 ppb on an annual mean basis and by a larger amount in JJA (12 to 37 ppb) over the major northern anthropogenic source regions since 1850, driven mainly by the large increases in anthropogenic precursor emissions of $CH_4$, $NO_x$, CO, and NMVOCs over this period.

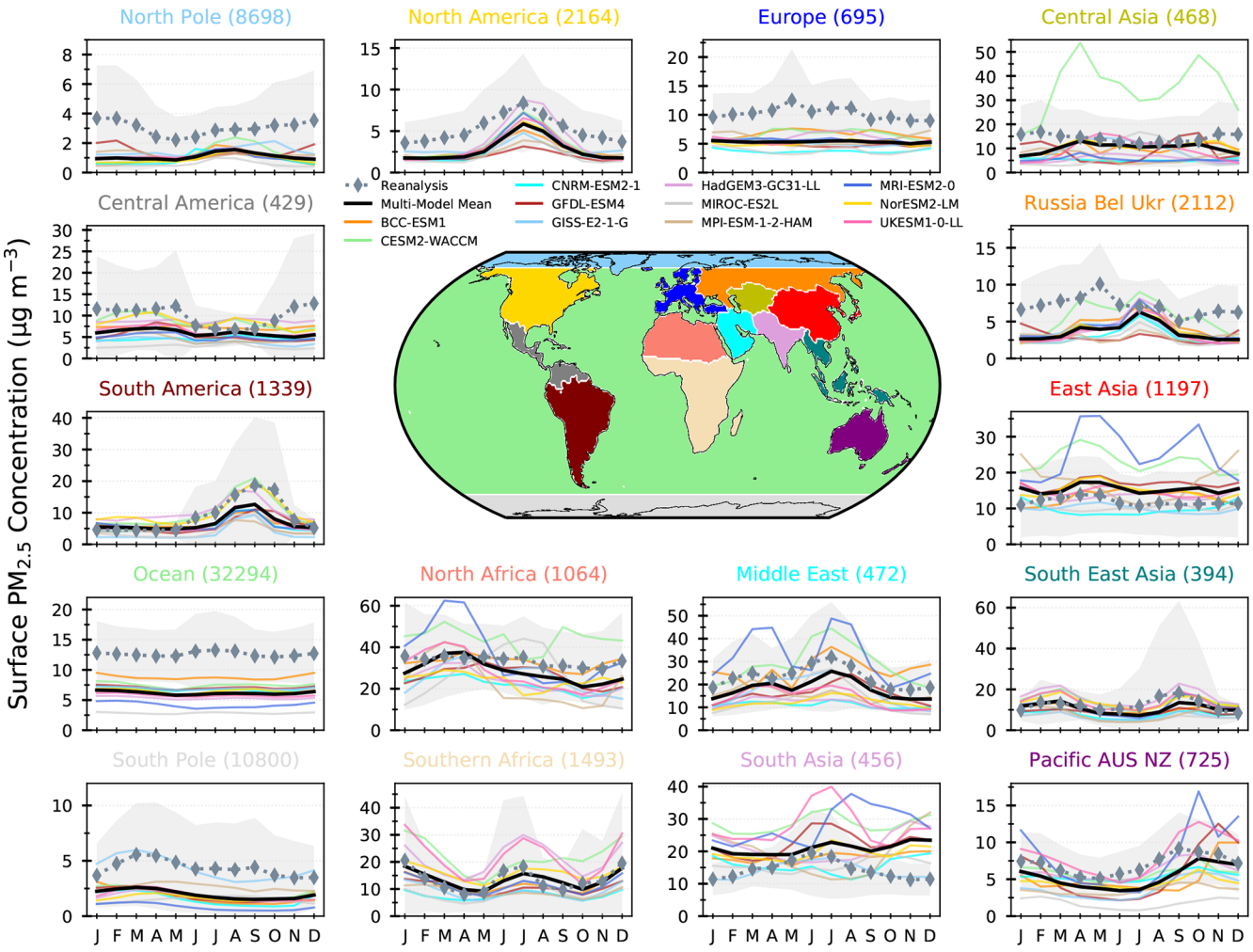


**Figure 8.** Individual and multi-model (11 CMIP6 models) monthly mean surface $PM_{2.5}$ concentrations across different world regions compared with the regional monthly values from the $PM_{2.5}$ MERRA-2 reanalysis within the region for the period 2005–2014. The number of reanalysis points within the region is shown in parentheses. The shading shows variability in the values of the MERRA-2 reanalysis products across the region.

A qualitative estimate of the influence of non-emission-driven processes (chemistry and climate change) can be ascertained by comparing results from the HTAP_param, an emission-only-driven model, to those of the CMIP6 models. Simulated historical changes in surface $O_3$ from UKESM1-0-LL are comparable to those from the HTAP_param, indicating that the magnitude of change simulated by UKESM1-0-LL is similar to that solely from changes in precursor emissions. However, the global annual mean surface $O_3$ response of $7.6 \pm 0.7$ ppb from HTAP_param over the historical period is 4.1 ppb lower than the CMIP6 multi-model mean, indicating globally that non-emission-driven processes have contributed to approximately 30 % of the change in surface $O_3$, although this contribution varies regionally. The different magnitude of response across models could be due to non-emission-driven processes, e.g. from different chemistry schemes and climate change signals within models.

## 4.2 Surface $PM_{2.5}$

The simulated change in annual mean surface $PM_{2.5}$ across 11 CMIP6 models is shown in Fig. 10 over the historical period of 1850 to 2014. CMIP6 models simulated an increase in global annual and seasonal mean surface $PM_{2.5}$ concentrations of $< 2\,\mu g\,m^{-3}$ (15 %–20 %) since 1850. Larger regional increases in surface annual mean $PM_{2.5}$ of up to $12\,\mu g\,m^{-3}$ are simulated across South and East Asia, with changes in DJF (up to $21\,\mu g\,m^{-3}$) larger than those in JJA (up to $12\,\mu g\,m^{-3}$; Fig. S16), reflecting the strong seasonality of $PM_{2.5}$ concentrations in these regions. The historical increase in surface $PM_{2.5}$ is primarily driven by the large increase in anthropogenic aerosol and aerosol precursor emissions over the 1850–2014 period (Hoesly et al., 2018). The largest model diversity is also exhibited over the Asian regions, with variations in the response between models of

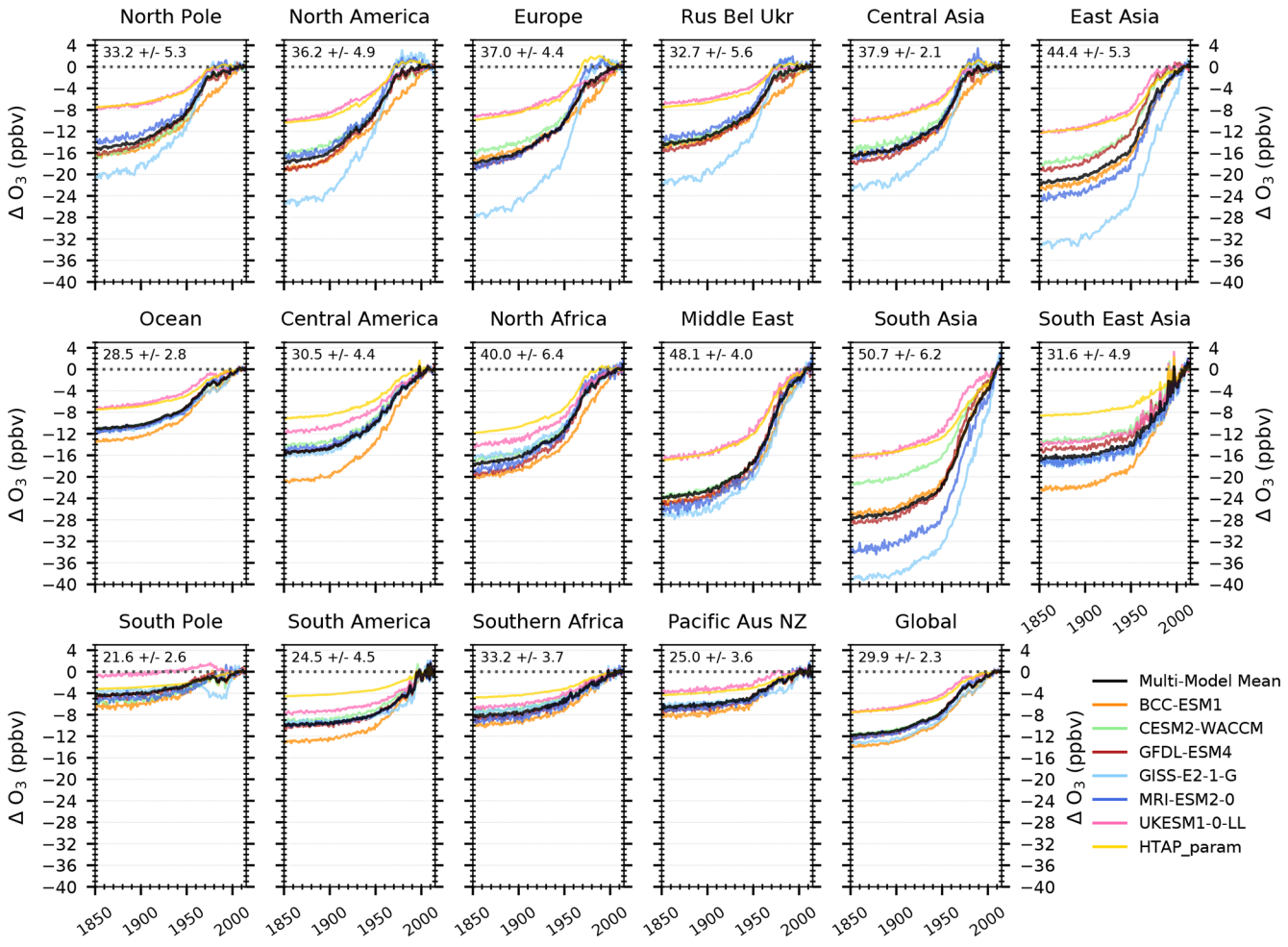


**Figure 9.** Changes in the regional and global annual mean surface $O_3$ concentrations, relative to a 2005–2014 mean value, across six CMIP6 models and the HTAP_param. The multi-model annual mean 2005–2014 surface $O_3$ concentrations (±1 SD) are shown in the top left of each panel. Regions are defined in Fig. S1.

up to 50 % and larger differences between models in DJF than JJA (Fig. S16), reflecting the differences shown in the present-day model evaluation (Fig. 6). The inter-model differences can be attributed to the different simulation of historical changes in the anthropogenic components sulphate, black carbon and organic aerosols (Fig. S18). The largest inter-annual variability in surface $PM_{2.5}$ concentrations occurs over the North African and Middle East regions as they are located near large sources of dust, whose emissions are highly dependent on meteorological fluctuations (wind speed). Over Europe and to a lesser extent Russia, Belarus, Ukraine and North America, the increase in surface $PM_{2.5}$ concentrations since 1850 peaked in the 1980s at 4 $\mu g\,m^{-3}$ above the 2005–2014 mean value before decreasing over the last 30 years. There are limited long-term multi-decadal observational data available to assess changes in aerosols simulated by global models. Previous studies using long-term data since the 1980s, mainly over Europe and North America, have found that global models are able to reproduce the observed multi-decadal changes in aerosols relatively well (Pozzoli et al., 2011; Leibensperger et al., 2012; Tørseth et al., 2012; Chin et al., 2014; Turnock et al., 2015; Aas et al., 2019). More recently, global composition models, including some CMIP6 models, were shown to be able to reproduce the observed changes in AOD, sulphate and particulate matter over the last 2 decades (Mortier et al., 2020). The ability of global composition models to reproduce historical changes in aerosols provides a degree of confidence in the future projections under the CMIP6 scenarios. Further model observational comparisons of multi-decadal changes in aerosols will need to be undertaken to improve the understanding of changing aerosol properties and processes.

## 5 Air pollutants from present day to 2100

An analysis is now made of the future projections of air pollutants in the CMIP6 Tier 1 scenarios, including ssp370-

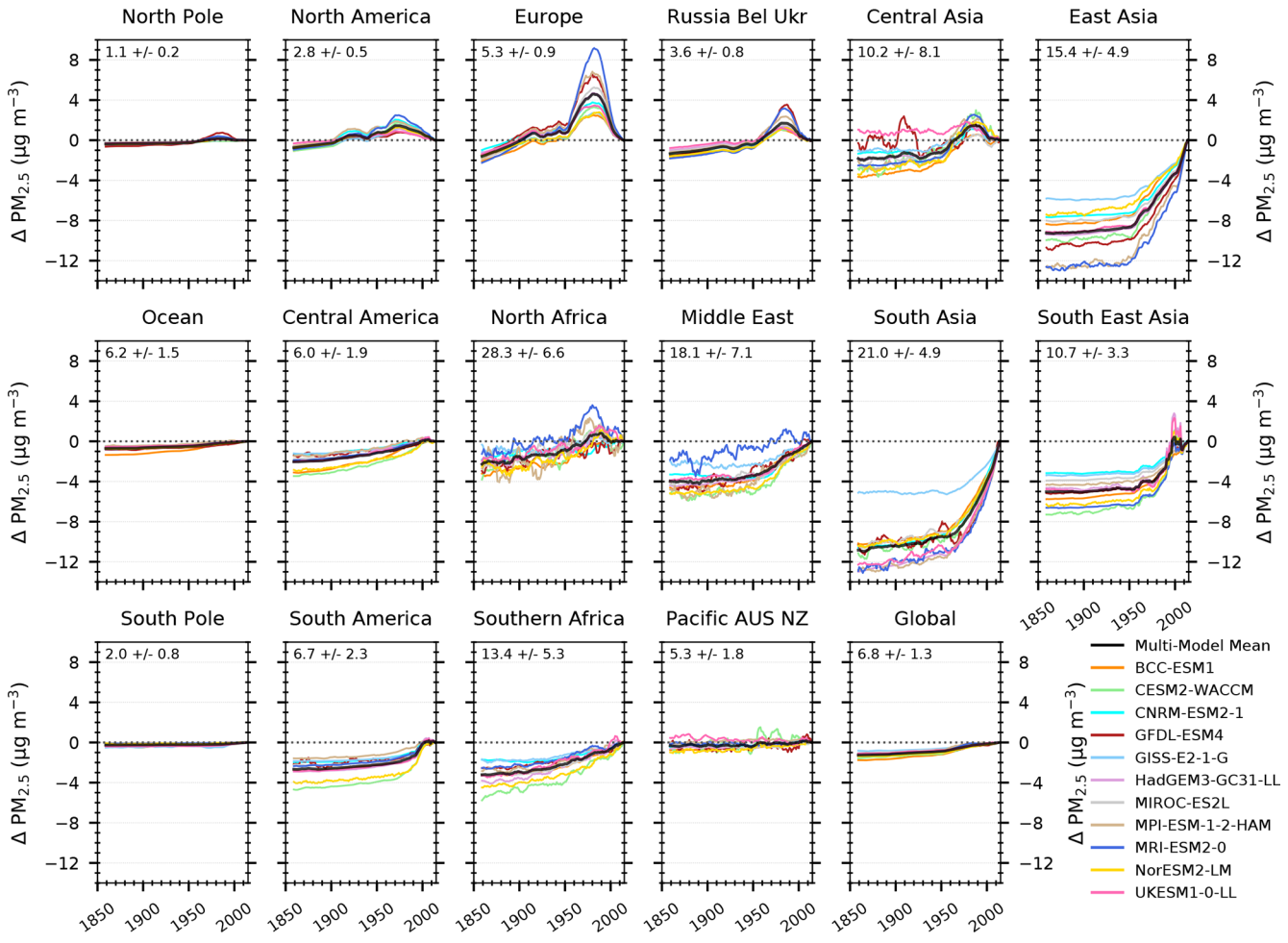


**Figure 10.** Changes in the regional and global annual mean surface $PM_{2.5}$ concentrations, relative to a 2005–2014 mean value, across 11 CMIP6 models. Changes for each region are computed as 10-year running means over the historical period. The multi-model mean 2005–2014 surface $PM_{2.5}$ concentrations (±1 SD) are shown in the top left of each panel. Regions are defined in Fig. S1.

lowNTCF. A comparison is made of the projected future changes in 2050 and 2100 from the four CMIP6 models (CESM2-WACCM, GFDL-ESM4 and UKESM1-0-LL for both $O_3$ and $PM_{2.5}$ along with BCC-ESM1 for $O_3$ and MIROC-ES2L for $PM_{2.5}$) that had the most data available for the ssp370 scenario.

### 5.1 Surface ozone

Global annual mean surface $O_3$ is reduced by more than $5 \pm 1.2$ ppb (±1 SD value of the multi-model mean) in the near-term (2050) and by $9 \pm 1.6$ ppb in 2100 in the strong air pollutant and climate mitigation scenario ssp126 (Fig. 11). Smaller reductions in global annual mean surface $O_3$ of $4 \pm 1.7$ ppb are predicted for the middle-of-the-road pathway (ssp245) by 2100, whereas for the weak climate and air pollutant mitigation scenario ssp370, a global annual mean increase in surface $O_3$ of 1.6±0.9 ppb in 2050 and 0.6±1.0 ppb by 2100 is predicted. However, implementing strong emission controls for SLCFs on top of a weak climate mitigation scenario (ssp370-lowNTCF) shows that previous increases in global annual mean surface $O_3$ can be substantially reduced to values that are $2.5 \pm 0.5$ ppb below the 2005–2014 mean value in 2050, with benefits to air quality and climate (Allen et al., 2020). For ssp585, which has weak climate mitigation measures but strong air pollution controls, a near-term increase in global annual mean surface $O_3$ of $1.4 \pm 0.8$ ppb is predicted in 2050, but by 2100 surface $O_3$ reduces by $2.7 \pm 1.5$ ppb, relative to 2005–2014, due to the implementation of air pollutant controls in the latter half of the 21st century.

The global response in annual mean surface $O_3$ concentrations to the different scenarios is also repeated across the different world regions, albeit with differing magnitudes. In ssp370, increases in annual mean surface $O_3$ are predicted to occur across North America (+1.6 ppb), Europe (+5.4 ppb) and East Asia (+5.9 ppb), with the largest increase, of 15.1 ± 9.6 ppb, predicted in South Asia by 2100. Despite the re-

ductions in $O_3$ precursor emissions across North America, Europe and East Asia by 2100 (Fig. 2), surface $O_3$ concentrations have continued to increase up to the end of this period, indicating the importance of future changes in chemistry, global $CH_4$ abundances and climate to the response of surface $O_3$ in ssp370 (Wild et al., 2012; Gao et al., 2013; Rasmussen et al., 2013; Young et al., 2013; Colette et al., 2015; Fortems-Cheiney et al., 2017; Li et al., 2019; Turnock et al., 2019). South Asia shows the largest increase in surface $O_3$ as precursor emissions are anticipated to increase across this region on top of the large climate change signal and growth in $CH_4$ abundance. Additionally, the largest diversity in projections between the CMIP6 models is shown over South Asia, indicating that there is some disagreement between the models as to the magnitude and extent of changes over this region. Surface $O_3$ across oceanic regions (background) is predicted to remain at or near current values in ssp370 due to the increases in water vapour in a warming world, leading to more $O_3$ destruction (Johnson et al., 1999; Doherty et al., 2013). The impact of more aggressive near-term reductions to emissions of SLCFs (but not $CH_4$) on top of the ssp370 pathway is shown by the smaller changes in the ssp370-lowNTCF (Figs. 11 and S19–S20 for individual models). In this pathway, surface $O_3$ concentrations are reduced globally and across most regions to be at or near 2005–2014 values, a substantial benefit to surface $O_3$ air quality compared to ssp370. Surface $O_3$ concentrations are predicted to have almost halved by 2050 across South Asia in ssp370-lowNTCF. However, across East Asia the additional precursor emission reductions in ssp370-lowNTCF have resulted in smaller benefits to surface $O_3$ concentrations being simulated by the CMIP6 models than in other regions (Fig. S20), which is attributed to an increase in surface $O_3$ concentrations over eastern China (a part of the larger East Asian region shown in Fig. S1). This increase in surface $O_3$ results from the slight increase in NMVOC emissions (Fig. 2) and a reduction in the $NO_x$ titration of $O_3$ due to the large decreases in $NO_x$ emissions in ssp370-lowNTCF. In addition, a reduction in the heterogeneous loss of radicals due to decreases in $PM_{2.5}$ concentrations in ssp370-lowNTCF could also lead to increased surface $O_3$ concentrations (Li et al., 2019).

Surface $O_3$ concentrations predicted across Northern Hemisphere regions in ssp585 are similar to ssp370 due to comparable changes in air pollutant emissions and climate change. However, a notable exception is a reduction in surface $O_3$ across regions towards the latter half of the 21st century (post-2080), when there are additional reductions in precursor emissions and global $CH_4$ abundances by 2100. Surface $O_3$ shows a slightly slower increase until the mid-21st century over South Asia in ssp585 than what occurred in ssp370. This can be attributed to a slightly different temporal evolution of $NO_x$ emissions over this region in that they peak earlier (by 2040) and decline more rapidly in ssp585 when compared to the continual increase in $NO_x$ emissions in ssp370 (Fig. 2), which results in a different response of $O_3$ formation within CMIP6 models, In addition, there are more CMIP6 models with data available for ssp370 (six models) than ssp585 (four models; Table 1), which could affect the multi-model mean response shown in Fig. 11.

The future scenario ssp245 (middle of the road) predicts annual mean surface $O_3$ concentrations that tend to remain at or near the 2005–2014 mean values by 2100 across the major anthropogenic source regions of the Northern Hemisphere, whereas for other tropical and Southern Hemisphere regions surface $O_3$ concentrations are reduced by more than 4 ppb. The changes in ssp245 are driven by larger precursor emission controls, a smaller climate change signal and controlling $CH_4$ so that global abundances are below 2015 values by 2100 (Fig. 1g). In ssp245 a near-term (up to 2040) increase in surface $O_3$ is shown across East Asia and South Asia, which could be attributed to the peaking of global $CH_4$ abundances at this point prior to then reducing.

The Tier 1 future scenario with the strongest climate and air pollutant mitigation measures, ssp126, shows substantial decreases in surface $O_3$ concentrations across most regions due to the large reduction in precursor emissions, global $CH_4$ abundances and small climate change signal. Reductions in surface $O_3$ of more than 10 ppb are predicted across anthropogenic-emission source regions of the Northern Hemisphere, with smaller reductions across Southern Hemisphere regions.

Projections from the CMIP6 models show that to achieve global benefits for regional surface $O_3$, it is important to control $O_3$ precursor emissions (including $CH_4$) in addition to limiting future climate change. However, scenarios with large climate change signals (ssp370 and ssp585) but different post-2050 controls on $O_3$ precursors (most notably $CH_4$ and $NO_x$) show different long-term changes in regional surface $O_3$ concentrations, which could have important consequences for any potential human health impacts.

A more detailed comparison of future surface $O_3$ projections between CMIP6 models has been undertaken for ssp370 as it is the scenario with the largest number of available models (Table 1). The regional change in annual and seasonal mean surface $O_3$, relative to 2005–2014, in 2050 (2045–2055 mean) and 2095 (2090–2100 mean) for ssp370 from four CMIP6 models and the HTAP_param is shown in Fig. 12. An analysis of the relationships, in terms of correlation coefficients, between future annual mean surface $O_3$ concentrations and other variables ($CH_4$ concentrations, surface air temperature, $NO_x$ concentrations, emissions of BVOCs and anthropogenic emissions of NMVOCs) is undertaken for CMIP6 models in the ssp370 scenario (Fig. 13). Discrepancies in the simulated response of background $O_3$ across the ocean region (as well as the South Pole and Pacific, Australia and New Zealand) are noticeable between individual models, with UKESM1-0-LL predicting a decrease in surface $O_3$ compared to the small increase from the HTAP_param and most other models in both 2050 and 2095 (Fig. S19). The future surface $O_3$ response in UKESM1-0-

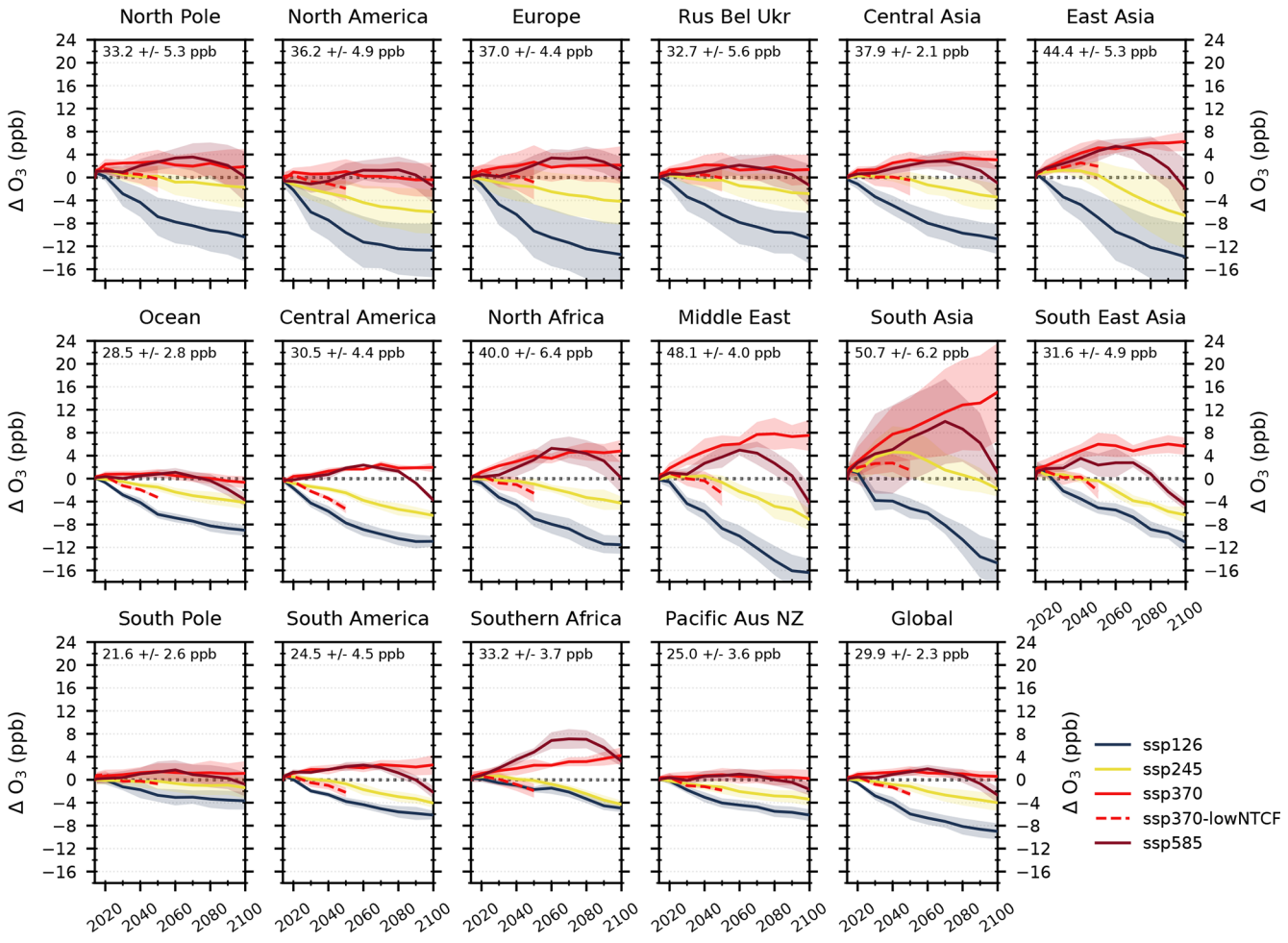


**Figure 11.** Future global and regional changes in annual mean surface $O_3$, relative to 2005–2014 mean, for the different SSPs used in CMIP6. Each line represents a multi-model mean across the region, with shading representing the ±1 SD of the mean. See Table 1 for details of models contributing to each scenario. The multi-model regional mean value (±1 SD) for the years 2005–2014 is shown in the top left corner of each panel.

LL over the ocean region exhibits a large negative correlation with surface temperature changes (Fig. 13), indicating the importance of future climate change in this model over remote regions. UKESM1-0-LL is a model with high equilibrium climate sensitivity (ECS; 5.4 K) compared to other CMIP6 models (Forster et al., 2019; Sellar et al., 2019) and therefore will exhibit a larger climate response (surface temperature and water vapour), leading to enhanced background $O_3$ destruction via water vapour and the hydroxyl radical (OH). Over the North Pole region all models show surface $O_3$ increases that are larger than the HTAP_param, with a larger increase in DJF than JJA. The large future temperature response over the Arctic and changes in $NO_x$ concentrations and emissions of NMVOCs are particularly important drivers of surface $O_3$ changes across most CMIP6 models in this region with comparatively low local emissions (Fig. 13).

Differences in the predicted surface $O_3$ between models exist across South Asia, where CESM2-WACCM (and BCC-ESM1 in 2050) predicts a response that is twice as large as UKESM1-0-LL and GFDL-ESM4. The lower annual mean response over South Asia in UKESM1-0-LL and GFDL-ESM4 is driven by a reduction in DJF in these models (Fig. S21), which results in the DJF change in 2050 being lower than the 2005–2014 annual mean value (Fig. 12). The large increase in $NO_x$ emissions in ssp370 over South Asia (∼ 80 %) has resulted in areas of $NO_x$ titration, particularly in DJF, near the Indo-Gangetic Plain in both UKESM1-0-LL and GFDL-ESM4, reducing surface $O_3$ concentrations (Figs. S19 and S21). This strong feature of $NO_x$ titration of $O_3$ in DJF is absent in both CESM2-WACCM and BCC-ESM1, resulting in larger $O_3$ production over South Asia. The comparison in Fig. 12 shows how the $O_3$ chemistry within models responds differently across a particular area in a future scenario with a large climate change signal and over a region with large increases in local precursor emissions but that all

the drivers related to regional $O_3$ change in South Asia are similarly important across all models (Fig. 13).

Over South America and Southern Africa, particularly the tropical areas (Fig. S19), larger future changes in surface $O_3$, particularly by 2100, are predicted by GFDL-ESM4 and UKESM1-0-LL than by CESM2-WACCM. These changes over South America are larger in JJA in all models, with small seasonal differences over Southern Africa. Over this region, biogenic emissions (particularly isoprene) are an important source of $O_3$ formation. Discrepancies in the future response of these BVOC emissions between models could be occurring due to the differing magnitudes of climate and land-use change and how they are coupled within individual CMIP6 models (Table S1), which could affect future surface $O_3$. Future changes in the total emissions of BVOCs and those solely from isoprene obtained from five CMIP6 models (Figs. S22 and S23) show that CESM2-WACCM has larger total BVOC emissions over the period 2005–2014 (due to the inclusion of more BVOCs), which then increase in the future ssp370 scenario, along with isoprene emissions, resulting in a smaller increase (and even decrease in some parts of the region) in $O_3$. In contrast, UKESM1-0-LL shows a larger increase in $O_3$ and a reduction in BVOC emissions, mainly from isoprene (Fig. 23), over parts of South America and tropical Africa. Figure 13 shows that there are differing relationships between future surface $O_3$ concentrations, BVOC emissions and $NO_x$ concentrations across CMIP6 models over South America and Southern Africa. Over Southern Africa, UKESM1-0-LL shows a different relationship between BVOC emissions and surface $O_3$ concentrations than other CMIP6 models, indicating that this could be leading to the different future $O_3$ response in this model over this region. Similarly, Fig. 13 shows that over South America, CESM2-WACCM has a different relationship between surface $O_3$ and the variables considered here than in other CMIP6 models, particularly for BVOCs, leading to the different future responses in this model over this region. Figure 13 shows that there are differences between models in the surface $O_3$ response over regions such as South America and Southern Africa, which are potentially linked to the land-surface response and are important to understand more in future work.

Whilst there are disagreements between models over some regions, there is also substantial consistency in the predicted increase in annual mean surface $O_3$ in ssp370 over North America, Europe and East Asia, which is larger than that from HTAP_param. However, BCC-ESM1 tends to predict a larger increase than the other three models, potentially due to the coarser resolution of this ESM. There are differences in simulated seasonal response across these regions, with all models showing a smaller increase in JJA than DJF across North America and Europe, whilst across East Asia there tends to a be a larger future surface $O_3$ increase in JJA than DJF. Figure 13 shows that there is a negative correlation between surface $O_3$ and $NO_x$ concentrations as well as between $O_3$ and NMVOC emissions for most CMIP6 models across these regions, reflecting that, as most anthropogenic precursor emissions (including $NO_x$) decrease in this scenario (Fig. 2), surface $O_3$ is simulated to increase. An exception to this is across East Asia, where the increase in NMVOC emissions in ssp370 (Fig. 2) is positively correlated with surface $O_3$, indicating different chemical drivers of future $O_3$ across this region. In addition, there are positive correlations between the other variables (temperature, $CH_4$ and BVOCs) for most CMIP6 models, indicating that changes in climate and global $CH_4$ abundances are also important drivers of surface $O_3$ increases over these regions.

The differences between the individual CMIP6 models highlight the importance of further understanding how future $O_3$ chemistry is affected by changes to precursor emissions and climate. The predicted differences in models can be quite pronounced over regions like South Asia, where changes in one model can be double that of another model, which could have important consequences for the ability of models to simulate future regional air quality.

### 5.2 Surface $PM_{2.5}$

Relatively small global changes in annual mean surface $PM_{2.5}$ are predicted for all CMIP6 models across all scenarios (Fig. 14), with an increase in ssp370 and a reduction in the others. Small reductions in $PM_{2.5}$ are predicted for all scenarios across Europe (0.3 to 3 $\mu g\,m^{-3}$) and North America (0.0 to 1.3 $\mu g\,m^{-3}$) due to the reduction in aerosol and aerosol precursor emissions. Differences in $PM_{2.5}$ between scenarios are highlighted across a number of regions.

For the weak climate and air pollutant mitigation scenario ssp370, increases in annual mean surface $PM_{2.5}$ are predicted across South Asia ($7.3 \pm 4.1\,\mu g\,m^{-3}$ by 2050 and $3.1 \pm 3.1\,\mu g\,m^{-3}$ by 2100), South East Asia ($2.7 \pm 4.7\,\mu g\,m^{-3}$ by 2100), Southern Africa ($1.6 \pm 3.7\,\mu g\,m^{-3}$ by 2100), Central America ($2.8 \pm 3.2\,\mu g\,m^{-3}$ by 2100) and South America ($2.9 \pm 3.6\,\mu g\,m^{-3}$ by 2100). The increases in $PM_{2.5}$ are driven mainly by the increase in aerosol and aerosol precursor emissions in this scenario (Fig. 2), shown by the positive correlations between emissions and surface $PM_{2.5}$ in CMIP6 models across these regions (Fig. 16). However, there is a degree of uncertainty associated with all of these future projections, indicated by the large diversity across the CMIP6 models. Some of the largest predicted increases in surface $PM_{2.5}$ occur across South Asia in ssp370, a region with already high present-day $PM_{2.5}$ concentrations. The increase in $PM_{2.5}$ peaks in 2050 across this region, which coincides with the increase in $SO_2$, BC and OC emissions before declining to 2100, when emissions reduce. Over East Asia, annual mean $PM_{2.5}$ concentrations are simulated to remain at or near 2005–2014 values until the latter half of the 21st century, when the decrease in emissions reduces $PM_{2.5}$ concentrations by $2.5 \pm 2.7\,\mu g\,m^{-3}$. The impact of reductions in SLCFs on top of the ssp370 scenario acts to constrain any increases

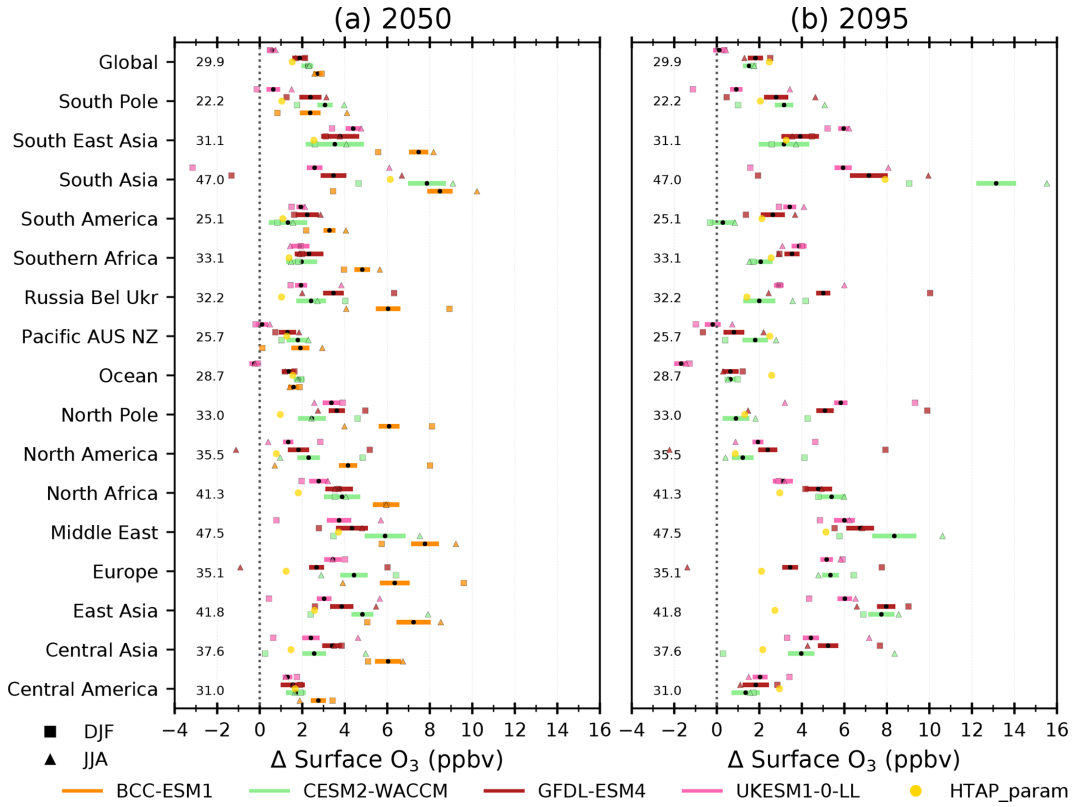


**Figure 12.** Future global and regional changes in the annual and seasonal mean surface $O_3$, relative to the 2005–2014 mean, for the ssp370 pathway used in CMIP6. Each black circle represents the annual mean response for an individual model in **(a)** 2045–2055 and **(b)** 2090–2100, with the coloured bars showing the SD across the annual mean. The DJF and JJA seasonal mean response averaged over the relevant 10-year period is shown by squares and triangles, respectively. The multi-model regional mean over the period 2005–2014 is given towards the left of each panel. The response from the HTAP_param in each time period is shown by the separate gold circle.

in $PM_{2.5}$ concentrations to near present-day values across most regions. However, substantial reductions in $PM_{2.5}$ concentrations of $5.6 \pm 2.0\,\mu g\,m^{-3}$ and $5.3 \pm 2.1\,\mu g\,m^{-3}$ below 2005–2014 values are achieved by 2050 across East and South Asia, respectively, by implementing these measures. Due to the short lifetime of aerosols in the atmosphere, $PM_{2.5}$ concentrations respond rapidly to the large cuts in emissions that occur in ssp370-lowNTCF and show the benefits of targeting these emissions, although there could be a potential climate impact (Allen et al., 2020).

Reductions in annual mean surface $PM_{2.5}$ are simulated across all regions for ssp126, ssp245 and ssp585. Differences exist in the magnitude and timing of $PM_{2.5}$ reductions across regions linked to the changes in emissions. The largest reductions in $PM_{2.5}$ occur over South Asia in 2100 and range from $11.1 \pm 2.8\,\mu g\,m^{-3}$ in ssp126 to $8.6 \pm 2.9\,\mu g\,m^{-3}$ in ssp585, a substantial benefit to regional air quality. Similar benefits to $PM_{2.5}$ are achieved over East Asia by 2100, although the more rapid improvements occur over this region in the first part of the 21st century.

The response of $PM_{2.5}$ concentrations is more variable, with a larger diversity across CMIP6 models within regions that are close to natural aerosol emission sources. This is particularly noticeable over North Africa, where the variability across CMIP6 models in dust emissions from the Saharan source region (Fig. S8) results in an uncertain $PM_{2.5}$ response across this region. A similar response is also exhibited across the Middle East and Central Asia. The potential influence of BVOCs on SOA formation (Figs. S22 and S26) could also be contributing to the diversity in the CMIP6 model responses across the South America and Southern Africa regions.

The CMIP6 models show that future reductions in aerosols and aerosol precursors will lead to a decrease in surface $PM_{2.5}$ concentrations across most world regions and a benefit to regional air quality (and human health), consistent with that from CMIP5. However, if emissions are not controlled over economically developing regions such as South America, Asia and Africa, then surface $PM_{2.5}$ is anticipated to increase and worsen future regional air quality. Targeting emission reductions in SLCFs in the short term shows the potential for rapid improvements in surface $PM_{2.5}$ and air quality.

In a similar analysis to that for surface $O_3$, a more detailed comparison has been undertaken of four CMIP6 models predicting changes in annual and seasonal surface $PM_{2.5}$

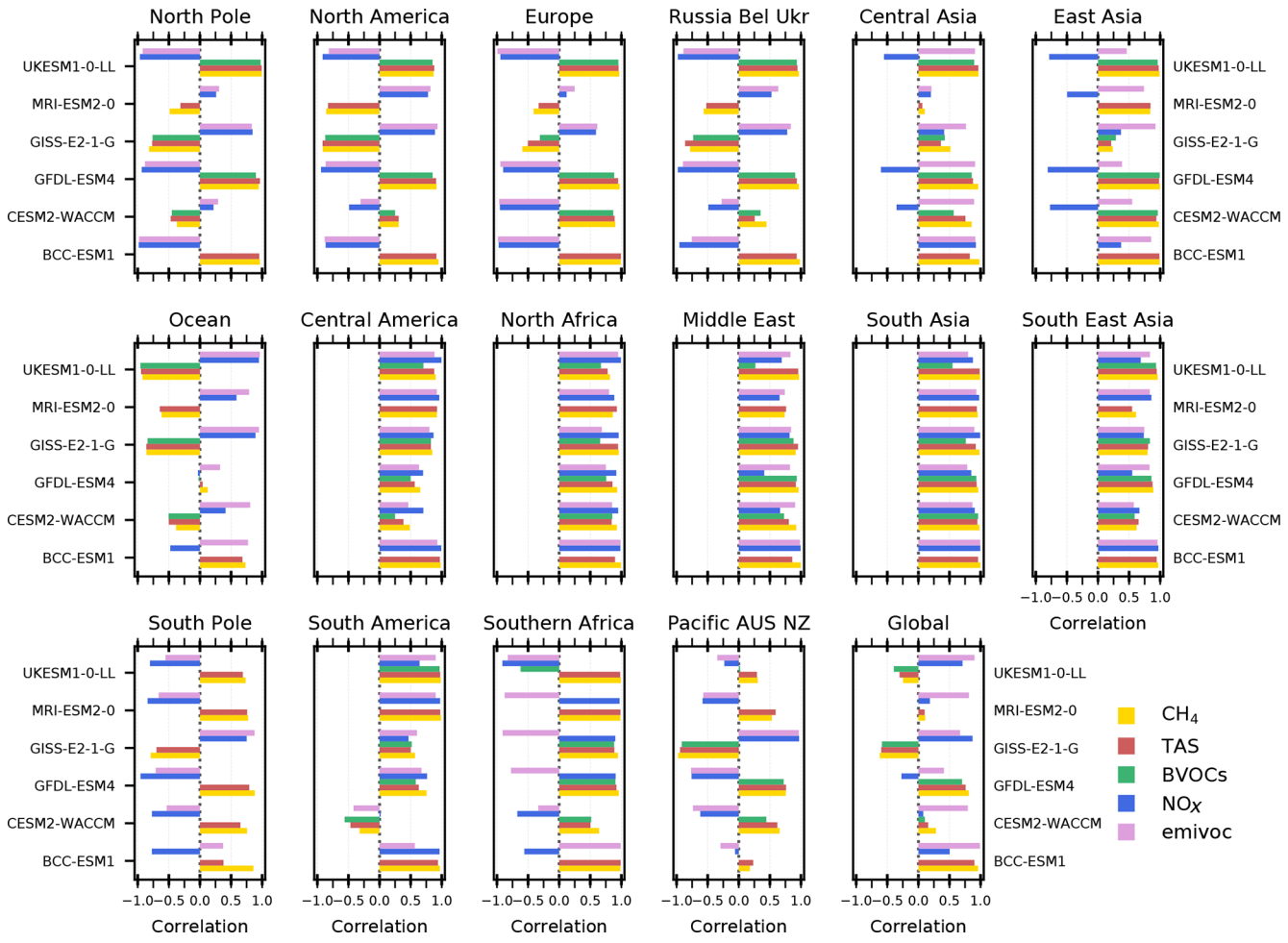


**Figure 13.** Correlation coefficients calculated when comparing future annual mean surface $O_3$ concentrations against individual variables of surface $CH_4$ concentrations, surface air temperature (TAS), emissions of biogenic volatile organic compounds (BVOCs), $NO_x$ ($NO + NO_2$) concentrations and anthropogenic emissions of non-methane volatile organic compounds (NMVOCs) from individual CMIP6 models over the period 2015 to 2100 in the ssp370 scenario.

in 2050 and 2095 under ssp370 (Fig. 15). In addition, an analysis of the relationships, in terms of correlation coefficients, between future annual mean surface $PM_{2.5}$ and other variables (total surface precipitation; surface air temperature; and emissions of BVOCs, $SO_2$, BC and organic aerosol) has been undertaken for CMIP6 models in the ssp370 scenario (Fig. 16). Small reductions in annual mean surface $PM_{2.5}$ concentrations ($< 2\,\mu g\,m^{-3}$) are simulated consistently by all CMIP6 models across North America and Europe in ssp370, with larger reductions simulated in DJF than JJA. The reductions in annual mean $PM_{2.5}$ over Europe and North America are mainly attributed to decreases in the BC and $SO_4$ components (Figs. S24 and S25), as indicated by the strong correlations with BC and $SO_2$ emissions across CMIP6 models (Fig. 16). However, by 2095 a small increase (up to $2\,\mu g\,m^{-3}$) is simulated in JJA by UKESM1-0-LL and CESM2-WACCM over North America, which could be attributed to changes in climate due to the strong positive correlations in both models for temperature, precipitation and BVOCs (Fig. 16).

South Asia, the region with the largest simulated future change in annual mean surface $PM_{2.5}$, of up to $12\,\mu g\,m^{-3}$, shows fairly good agreement between three CMIP6 models (UKESM1-0-LL, GFDL-ESM4 and CESM2-WACCM) as projections in 2050 and 2095 are all within the range of each of the individual models. The future increases in annual mean surface $PM_{2.5}$ appear to be strongly driven by emission changes as there are strong positive correlations between these variables across South Asia in all models (Fig. 16). Across South Asia, all models simulate a larger increase in DJF mean surface $PM_{2.5}$ concentrations, of up to $18\,\mu g\,m^{-3}$ by 2050, than what occurs in JJA, reflecting the seasonality shown in the model evaluation. The MIROC-ES2L model predicts smaller future increases in surface $PM_{2.5}$, of up to $5\,\mu g\,m^{-3}$, than the other models across South Asia in both 2050 and 2095. This is a result of smaller changes in the BC,

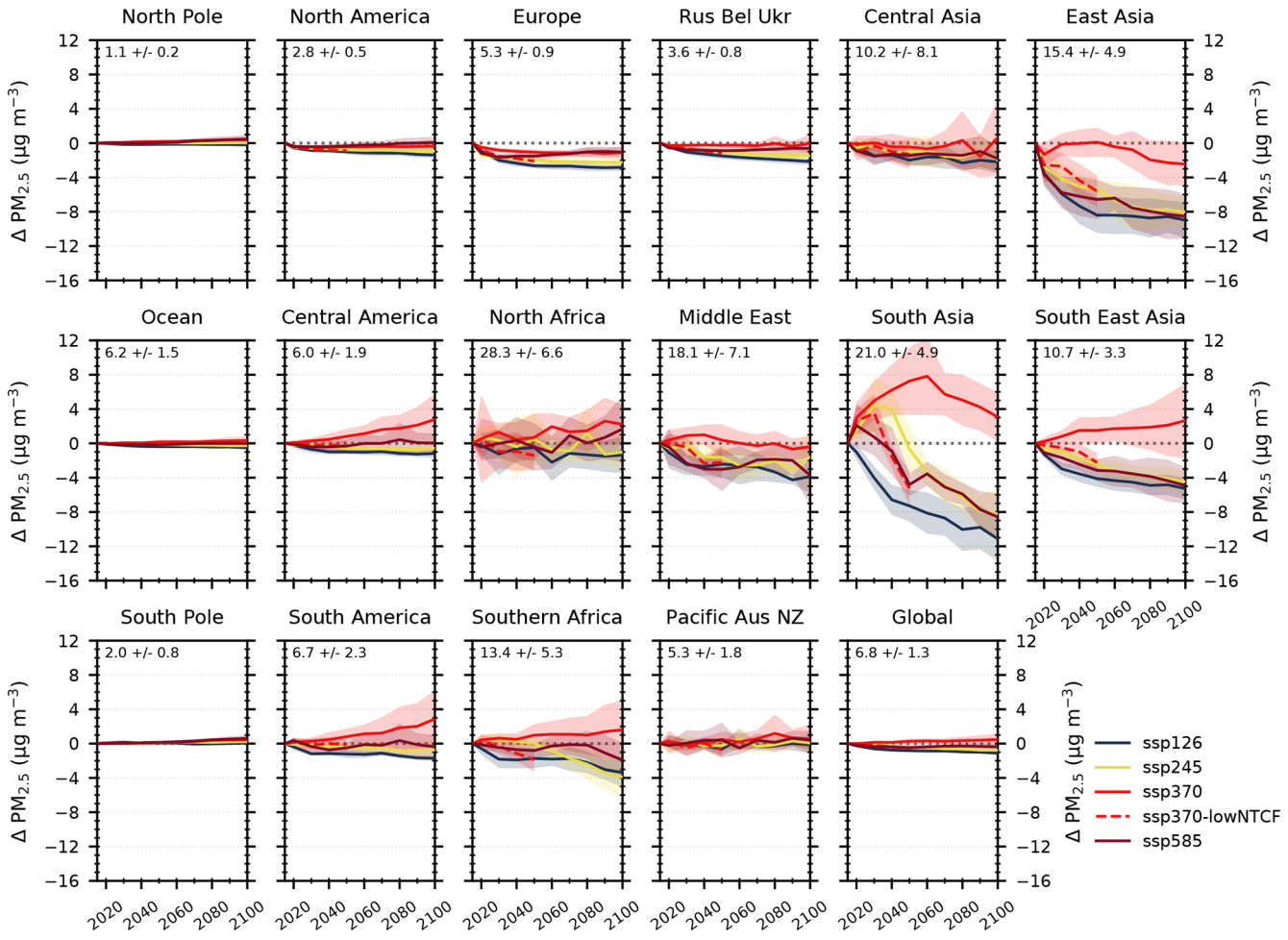


**Figure 14.** Future global and regional changes in annual mean surface $PM_{2.5}$, relative to 2005–2014 mean, for the different SSPs used in CMIP6. Each line represents a multi-model mean across the region, with shading representing the ±1 SD of the mean. See Table 1 for details of models contributing to each scenario. The multi-model regional mean value (±1 SD) for the years 2005–2014 is shown in the top left corner of each panel.

OA and sulphate aerosol components in the MIROC-ES2L model despite increases in aerosols and aerosol precursor emissions across South Asia in ssp370 (Fig. S24–S26).

Disagreements in both the sign and magnitude of simulated future annual and seasonal mean surface $PM_{2.5}$ changes between CMIP6 models are also exhibited across East Asia. Small regional annual mean increases are predicted in 2050 due to $PM_{2.5}$ increases in JJA from all models apart from GFDL-ESM4. A larger reduction in the $SO_4$ component is simulated over East Asia by GFDL-ESM4 than in other models (Fig. S25), resulting in an overall decrease in $PM_{2.5}$. In 2095 most models simulate a reduction in $PM_{2.5}$ concentrations in both seasons across East Asia, apart from CESM2-WACCM due to the increase in JJA. All models simulate continual reductions out to 2100 for $SO_4$ across this region, whereas BC increases in the near term before decreasing out to 2100. For OA, CESM2-WACCM shows larger increases over East Asia in both 2050 and 2095 compared to the other models, which show a smaller increase in 2050 and a reduction by 2095 (Fig. S26). CESM2-WACCM includes a more complex treatment of SOA formation, showing a strong response to climate and historical trends in OA (Tilmes et al., 2019). Positive correlations are shown for CESM2-WACCM between surface $PM_{2.5}$ and emissions of BVOC as well as between surface $PM_{2.5}$ and temperature (Fig. 16), which are not present in other models and could explain the differences between this model and others across East Asia. The discrepancies in CMIP6 models are not as obvious over South Asia as the effect of the increase in OA over South Asia in CESM2-WACCM is masked by coincident increases in other components across other models, as indicated by the strong correlations with emissions here. CESM2-WACCM also shows larger simulated increases in $PM_{2.5}$ over South America, Central America, Southern Africa and South East Asia than other models, which can be attributed to the larger increase in the OA fraction (Fig. S26) and the strong corre-

lations in this model with changes in temperature and emissions (BVOCs and $SO_2$). Over Southern Africa UKESM1-0-LL shows a reduction in future $PM_{2.5}$ in contrast to other models due to a reduction in the BC, OA and dust aerosol components (Figs. S24, S26 and S27). UKESM1-0-LL exhibits particularly strong negative correlations for surface $PM_{2.5}$ when compared with temperature and precipitation. These relationships over Southern Africa are quite different to other CMIP6 models, which is also highlighted in the model evaluation over this region (Fig. 8) and indicates that climate change influences aerosol concentrations differently over this region in this model (Fig. 16). In addition, there is a slight positive correlation of $PM_{2.5}$ with BVOC emissions in UKESM1-0-LL over Southern Africa. Future biogenic emissions (including monoterpenes) reduce here in ssp370 (Fig. S22), potentially due to land-use vegetation change as UKESM1-0-LL has dynamic vegetation coupled to BVOC emissions (Table S1 in the Supplement). This could also reduce $PM_{2.5}$ concentrations over this region because monoterpene emissions are the main precursor to SOA formation in UKESM1-0-LL (Mulcahy et al., 2020).

The annual and seasonal mean $PM_{2.5}$ response is variable across individual CMIP6 models over regions close to natural sources of particulate matter (North Africa; Central Asia; and Pacific, Australia and New Zealand). Over these regions there is a large range in both the sign and magnitude of the annual and seasonal $PM_{2.5}$ response, which can be mainly attributed to the dust fraction (Fig. S27) and the fact that this aerosol source has a large inter-annual variability in its emission strength. There is also a lack of consistency across CMIP6 models in the correlations of $PM_{2.5}$ with any individual driver, indicating the variability of aerosol sources in these regions within models. Interestingly, the CMIP6 models do not agree in the sign and magnitude of future changes to dust concentrations in ssp370 (Fig. S27).

Across the ocean and North Pole regions, all the CMIP6 models tend to simulate a small increase in $PM_{2.5}$ concentrations, which can be attributed to increases in sea salt concentrations (Fig. S28). A strong increase in sea salt concentrations is simulated in all models across the Southern Ocean (and other oceans), potentially driven by changes to meteorological conditions (reflected by the positive correlations of $PM_{2.5}$ with the climate variables temperature and precipitation in Fig. 16), which increase wind speed and sea salt emissions. As ssp370 is a scenario with a large climate change signal, the increases in $PM_{2.5}$ across the North Pole, particularly in 2100, can be attributed to the melting of sea ice increasing sea salt emissions, which again is reflected in the positive correlations of $PM_{2.5}$ with climate variables over this region. However, the magnitude of this response is different in the CMIP6 models due to the underlying ECS and the response of Arctic surface temperatures within the individual model.

The differences in the simulated future $PM_{2.5}$ changes across the CMIP6 models in ssp370 highlight that it is important to consider how natural sources of aerosol respond in a future climate in addition to changes from anthropogenic emissions. Particular differences between models have been shown for dust, sea salt and also organic (secondary) aerosols, which should be explored further. In addition, the different representations of aerosols within individual models, e.g. organic aerosols, are an important consideration as they can make a large difference to any future regional projection of $PM_{2.5}$.

## 6 Conclusions

In this study we have provided an initial analysis of the historical and future changes in air pollutants ($O_3$ and $PM_{2.5}$) from the latest generation of Earth system and climate models that have submitted results from experiments conducted as part of CMIP6. Data were available from the historical experiments of 6 CMIP6 models for surface $O_3$ and 11 models for surface $PM_{2.5}$. Historical changes in regional concentrations of $O_3$ and $PM_{2.5}$ are presented over the period 1850 to 2014 using data from all models. A present-day model evaluation of the CMIP6 models was conducted against surface observations of $O_3$ and $PM_{2.5}$ obtained from the TOAR and GASSP databases, respectively. An additional comparison was performed for simulated $PM_{2.5}$ concentrations against the MERRA-2 aerosol reanalysis product. An assessment is then made of the changes in surface $O_3$ and $PM_{2.5}$ simulated by the CMIP6 models across different future scenarios, ranging from weak to strong air pollutant and climate mitigation.

The six CMIP6 models simulate present-day (2005–2014) surface $O_3$ concentrations that are elevated in the Northern Hemisphere summer, with lower values throughout the year across the Southern Hemisphere. However, a large model diversity is shown across the continental Northern Hemisphere due to the large simulated seasonal cycles in certain models. Compared to surface $O_3$ measurements, CMIP6 models overestimate observed annual mean values and in both summer and winter across most regions by up to 16 ppb (a similar result to previous multi-model evaluations of global chemistry–climate models in Young et al., 2018). An exception to this is at observation locations across Antarctica, where CMIP6 models tend to underestimate observed values by 5 ppb.

Large surface $PM_{2.5}$ concentrations are simulated in CMIP6 models near dust and anthropogenic-emission source regions. Model diversity across the CMIP6 models is largest near the dust source regions due to their sensitivity to meteorological variability, whereas across other regions the CMIP6 models are relatively similar in their simulation of $PM_{2.5}$ concentrations. Evaluating the approximate $PM_{2.5}$ calculated from CMIP6 models (excluding nitrate aerosols) against ground-based $PM_{2.5}$ observations shows an underestimation across most regions of up to $10\,\mu g\,m^{-3}$. The underestimation of observations by models is larger in the Northern Hemi-

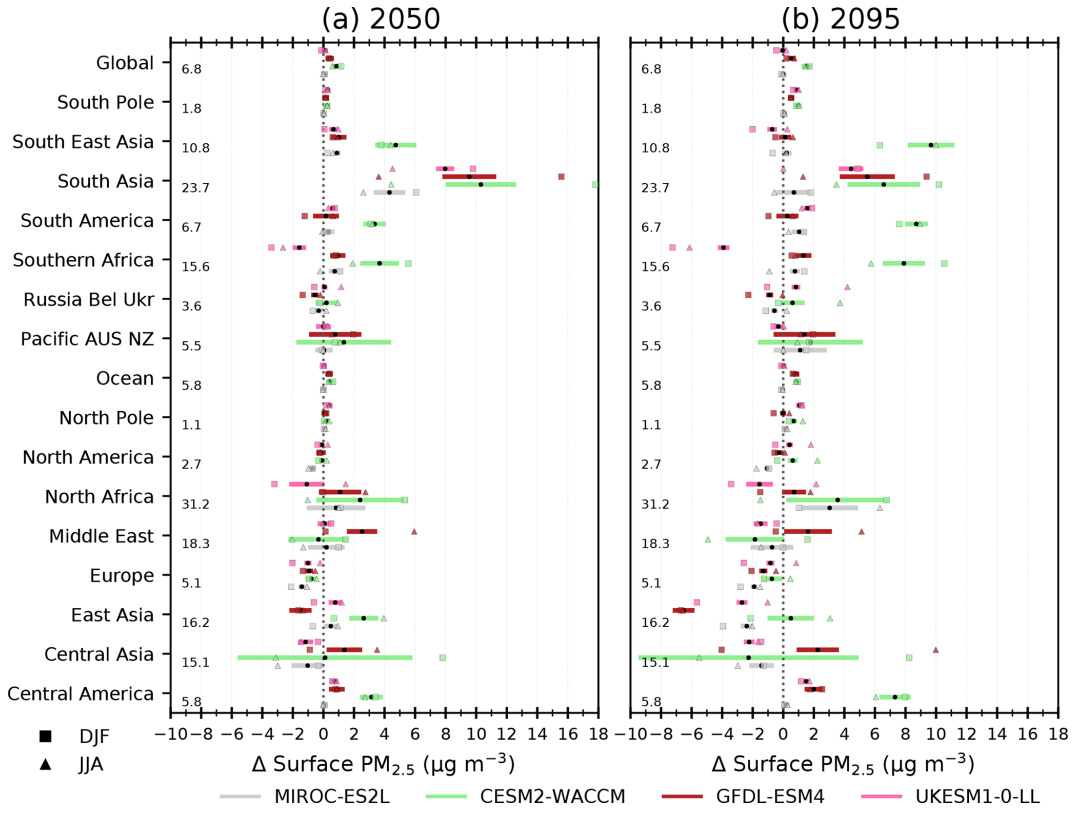


**Figure 15.** Future global and regional changes in the annual and seasonal mean surface $PM_{2.5}$, relative to the 2005–2014 mean, for the ssp370 pathway used in CMIP6. Each black circle represents the annual mean response for an individual model in **(a)** 2045–2055 and **(b)** 2090–2100, with the coloured bars showing the SD across the annual mean. The DJF and JJA seasonal mean responses averaged over the relevant 10-year periods are shown by squares and triangles, respectively. The multi-model regional mean over the period 2005–2014 is given towards the left of each panel.

sphere winter than summer, in part due to the absence of nitrate aerosols within most CMIP6 models and also due to underrepresentation of other aerosol processes within global models (a similar result to other multi-model assessments). To improve the spatial coverage and consistency of the $PM_{2.5}$ evaluation with CMIP6 models, an additional comparison was made to the MERRA-2 aerosol reanalysis product. A similar but slightly smaller underestimation of $PM_{2.5}$ concentrations over Europe and North America was found in the comparison of CMIP6 models and MERRA-2, providing further confidence in the result from the ground-based comparison. CMIP6 models overestimated the monthly $PM_{2.5}$ concentrations in MERRA-2 over South and East Asia by up to 15 $\mu g\,m^{-3}$, in contrast to the evaluation using ground-based observations. Mean annual cycles simulated by CMIP6 models and MERRA-2 tend to agree across other regions for which there are no suitable ground-based observations. The comparison of surface $O_3$ and $PM_{2.5}$ simulated by CMIP6 models to observations shows similar biases to previous generations of global composition–climate models. Further studies are required (e.g. global sensitivity or process studies) to explore uncertainties in models and the differences with observations.

Across the historical period (1850–2014), the CMIP6 models simulated a global annual increase in surface $O_3$ of between 7 and 14 ppb, with a larger increase in JJA than DJF. A global multi-model mean increase of $11.7 \pm 2.3$ ppb was simulated by the CMIP6 models, which agrees well with the change previously simulated by CMIP5 models. A large diversity in the historical change in surface $O_3$ was simulated by CMIP6 models across South Asia and other Northern Hemisphere regions. CMIP6 models predicted larger historical changes in surface $O_3$ than those from an emission-only-driven parameterisation, indicating a potential climate change impact (Wu et al., 2008; Bloomer et al., 2009; Weaver et al., 2009; Rasmussen et al., 2013; Colette et al., 2015) on surface $O_3$ over the historical period. Small global increases in surface $PM_{2.5}$ are simulated over the historical period by CMIP6 models, with larger regional changes of up to 12 $\mu g\,m^{-3}$ on an annual mean basis and up to 18 $\mu g\,m^{-3}$ in DJF across East and South Asia. The largest diversity in the response of CMIP6 models occurs over Asian regions, with large inter-annual variabilities near dust source regions.

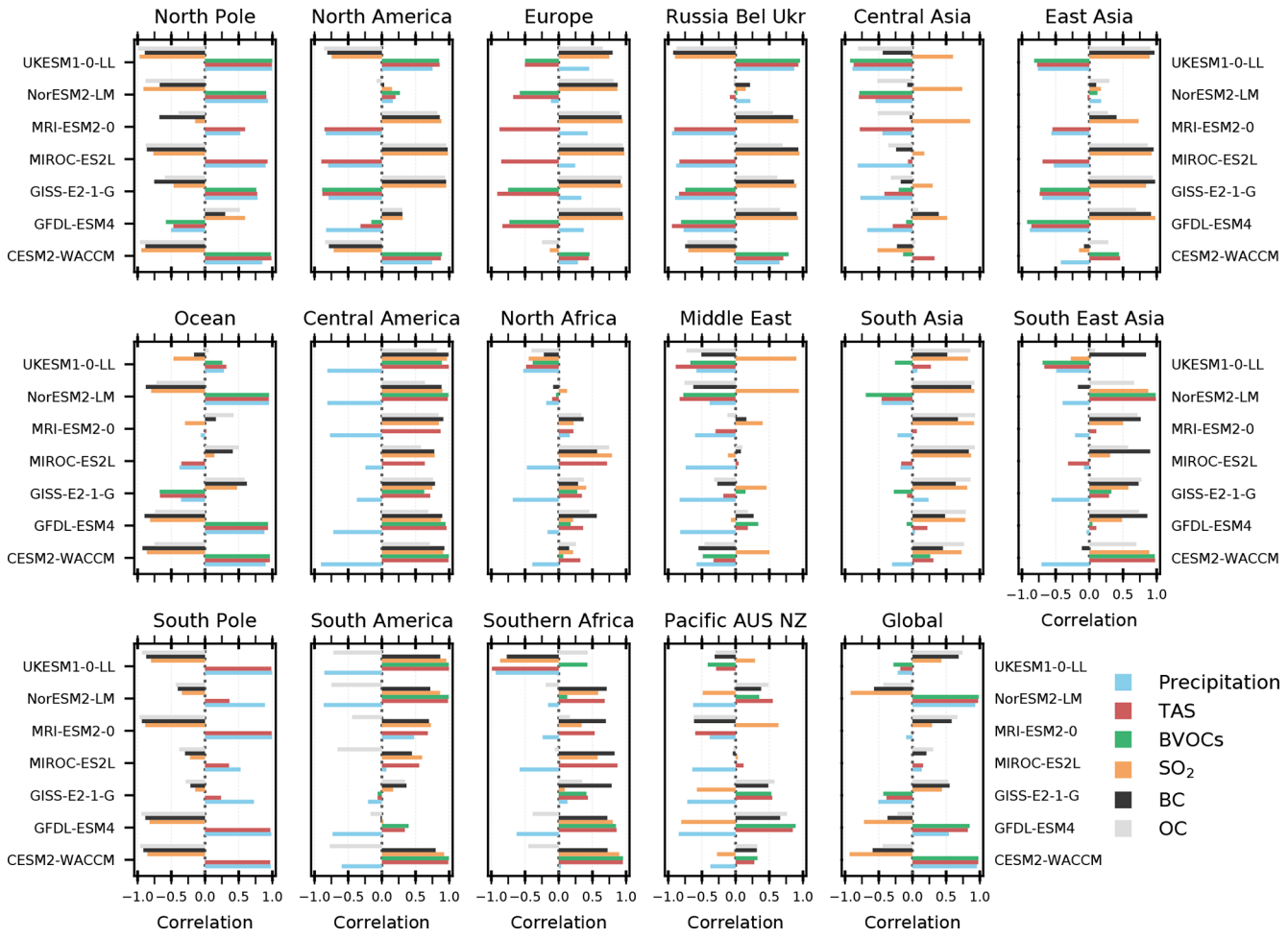


**Figure 16.** Correlation coefficients calculated when comparing future annual mean surface $PM_{2.5}$ concentrations against individual variables from individual CMIP6 models (that had data out to 2100) over the period 2015 to 2100 in the ssp370 scenario: precipitation; surface air temperature (TAS); emissions of biogenic volatile organic compounds (BVOCs); and emissions of $SO_2$, black carbon (BC) and organic carbon (OC).

CMIP6 models simulate the peak in $PM_{2.5}$ concentrations in the 1980s across Europe and North America prior to simulating the observed decline in concentrations to present day (Leibensperger et al., 2012; Tørseth et al., 2012; Turnock et al., 2015), attributed to the implementation of air pollutant emission controls over these regions.

The CMIP6 models predict that surface $O_3$ will increase across most regions in the weak-mitigation scenarios (ssp370 and ssp585), particularly over South and East Asia (up to 16 ppb by 2100) due to a combination of increases in air pollutant emissions, increases in global $CH_4$ abundances and climate change. Discrepancies exist in the regional surface $O_3$ response in ssp370 between individual CMIP6 models due to differences in the response of chemistry ($NO_x$; Fig. S17), climate (temperature) and biogenic precursor emissions (Fig. S22). Benefits to regional air quality from large reductions in surface $O_3$ are possible across all regions for scenarios that contain strong climate and air pollutant mitigation measures, including those targeting $CH_4$.

CMIP6 models predict that surface $PM_{2.5}$ concentrations will decrease across all regions in both the middle-of-the-road (ssp245) and strong-mitigation scenarios (ssp126) by up to 12 $\mu g\,m^{-3}$ due to the reduction in anthropogenic aerosols and aerosol precursor emissions, yielding a benefit to regional air quality, whereas for the weak climate and air pollutant mitigation scenario (ssp370), annual and seasonal mean surface $PM_{2.5}$ is simulated to increase across a number of regions. Implementing mitigation measures specifically targeting SLCFs on top of the ssp370 scenario shows immediate improvements in $PM_{2.5}$ concentrations, restricting any changes to below present-day values. The largest change in regional mean $PM_{2.5}$ concentrations and also largest diversity across CMIP6 models are predicted in ssp370 across South Asia, an area with already poor air quality. Disagreements in the projection of future changes to regional sur-

face $PM_{2.5}$ concentrations between individual CMIP6 models can be attributed to differences in the complexity of the aerosol schemes implemented within models, in particular the formation mechanisms of organic aerosols and emission of BVOCs over certain regions, along with the strength of the climate change signal (temperature and precipitation) simulated by models and the impact this has on natural aerosol emissions via Earth system couplings.

The results from CMIP6 provide an opportunity to assess the simulation of historical and future changes in air pollutants within the latest generation of Earth system and climate models using up-to-date scenarios of future socioeconomic development. Large changes in air pollutants were simulated over the historical period, primarily in response to changes in anthropogenic emissions. Future regional concentrations of air pollutants depend on the particular trajectory of climate and air pollutant mitigation that the world follows, with important consequences for regional air quality and human health. Substantial benefits can be achieved across most world regions by implementing measures to mitigate the extent of climate change as well as from large reductions in air pollutant emissions, including $CH_4$, which is particularly important for controlling $O_3$. In future scenarios which do not mitigate climate change and air pollutant emissions, the regional concentrations of air pollutants are anticipated to increase. Important differences between individual CMIP6 models have been identified in terms of how they simulate air pollutants from the interaction of chemistry ($O_3$ and $NO_x$), climate (temperature and precipitation) and natural precursor emissions (BVOCs) in the future. Further research and understanding of these processes are necessary to improve the robustness of regional projections of air pollutants on climate change timescales (decadal to centennial).

*Data availability.* CMIP6 data are archived at the Earth System Grid Federation and are freely available to download. The data on ESGF can be accessed via the website interface https://pcmdi.llnl.gov/CMIP6/ (last access: 8 September 2020, WCRP, 2020), and all the relevant references to the data used are provided in Table 1 as stated in the text.

*Supplement.* The supplement related to this article is available online at: https://doi.org/10.5194/acp-20-14547-2020-supplement.

*Author contributions.* STT conducted the analysis and wrote the paper with contributions from RJA. TW and JZ performed BCC-ESM1 simulations. LE and ST performed CESM2-WACCM simulations. PN and MM performed CNRM-ESM2-1 simulations. LH and JGJ performed GFDL-ESM4 simulations. SEB and KT performed GISS-E2-1-G simulations. MA and PG performed HadGEM3-GC31-LL simulations. TT performed MIROC6-ES2L simulations. DN performed MPI-ESM1.2-HAM simulations. MD and NO performed MRI-ESM2-0 simulations. DO and MS performed NorESM2-LM simulations. AS, FMO'C and SS performed UKESM1-0-LL simulations. All co-authors have been involved in providing comments and editing the manuscript.

*Competing interests.* The authors declare that they have no conflict of interest.

*Special issue statement.* This article is part of the special issue "The Aerosol Chemistry Model Intercomparison Project (AerChemMIP)". It is not associated with a conference.

*Acknowledgements.* For making their measurement data available to be used in this study, we would like to acknowledge the providers who supplied their data to the GASSP database and TOAR database.

Kostas Tsigaridis and Susanne E. Bauer acknowledge resources supporting this work provided by the NASA High-End Computing (HEC) programme through the NASA Center for Climate Simulation (NCCS) at Goddard Space Flight Center.

*Financial support.* Steven T. Turnock and Fiona M. O'Connor have been supported by the BEIS and DEFRA Met Office Hadley Centre Climate Programme (GA01101). Steven T. Turnock has been supported by the UK–China Research and Innovation Partnership Fund through the Met Office Climate Science for Service Partnership (CSSP) China as part of the Newton Fund. Fiona M. O'Connor has been supported by the EU Horizon 2020 research programme (CRESCENDO (grant agreement no. 641816)). Toshihiko Takemura has been supported by the supercomputer system of the National Institute for Environmental Studies, Japan, and JSPS KAKENHI (grant no. JP19H05669). Makoto Deushi and Naga Oshima have been supported by the Japan Society for the Promotion of Science (grant nos. JP18H03363, JP18H05292 and JP20K04070) and the Environmental Restoration and Conservation Agency of Japan through the Environment Research and Technology Development Fund (grant nos. JPMEERF20172003, JPMEERF20202003 and JPMEERF20205001). David Neubauer has been supported by the European Union's Horizon 2020 research and innovation programme project (FORCeS (grant agreement no. 821205)) and Deutsches Klimarechenzentrum (DKRZ; project ID 1051). Sungbo Shim has been supported by the Korea Meteorological Administration research and development programme "Development and Assessment of IPCC AR6 Climate change scenario" (grant no. KMA2018-00321).

*Review statement.* This paper was edited by Holger Tost and reviewed by two anonymous referees.

## References

Aas, W., Mortier, A., Bowersox, V., Cherian, R., Faluvegi, G., Fagerli, H., Hand, J., Klimont, Z., Galy-Lacaux, C., Lehmann, C. M. B., Myhre, C. L., Myhre, G., Olivié, D., Sato, K.,

Quaas, J., Rao, P. S. P., Schulz, M., Shindell, D., Skeie, R. B., Stein, A., Takemura, T., Tsyro, S., Vet, R., and Xu, X.: Global and regional trends of atmospheric sulfur, Sci. Rep., 9, 953, https://doi.org/10.1038/s41598-018-37304-0, 2019.

Allen, R. J., Landuyt, W., and Rumbold, S. T.: An increase in aerosol burden and radiative effects in a warmer world, Nat. Clim. Chang., 6, 269–274, https://doi.org/10.1038/nclimate2827, 2016.

Allen, R. J., Turnock, S., Nabat, P., Neubauer, D., Lohmann, U., Olivié, D., Oshima, N., Michou, M., Wu, T., Zhang, J., Takemura, T., Schulz, M., Tsigaridis, K., Bauer, S. E., Emmons, L., Horowitz, L., Naik, V., van Noije, T., Bergman, T., Lamarque, J.-F., Zanis, P., Tegen, I., Westervelt, D. M., Le Sager, P., Good, P., Shim, S., O'Connor, F., Akritidis, D., Georgoulias, A. K., Deushi, M., Sentman, L. T., John, J. G., Fujimori, S., and Collins, W. J.: Climate and air quality impacts due to mitigation of non-methane near-term climate forcers, Atmos. Chem. Phys., 20, 9641–9663, https://doi.org/10.5194/acp-20-9641-2020, 2020.

Apte, J. S., Marshall, J. D., Cohen, A. J., and Brauer, M.: Addressing Global Mortality from Ambient $PM_{2.5}$, Environ. Sci. Technol., 49, 8057–8066, https://doi.org/10.1021/acs.est.5b01236, 2015.

Bauer, S. E., Tsigaridis, K., Faluvegi, G., Kelley, M., Lo, K. K., Miller, R. L., Nazarenko, L., Schmidt, G. A., and Wu, J.: Historical (1850–2014) aerosol evolution and role on climate forcing using the GISS ModelE2.1 contribution to CMIP6, J. Adv. Model. Earth Syst., 12, e2019MS001978, https://doi.org/10.1029/2019ms001978, 2020.

Bloomer, B. J., Stehr, J. W., Piety, C. A., Salawitch, R. J., and Dickerson, R. R.: Observed relationships of ozone air pollution with temperature and emissions, Geophys. Res. Lett., 36, 1–5, https://doi.org/10.1029/2009GL037308, 2009.

Boucher, O., Randall, P., Artaxo, P., Bretherton, C., Feingold, G., Forster, P., Kerminen, V.-M., Kondo, Y., Liao, H., Lohmann, U., Rasch, P., Satheesh, S. K., Sherwood, S., Stevens, B., and Zhang, X. Y.: Clouds and Aerosols. In: Climate Change 2013: The Physical Science Basis. Contribution of Working Group I to the Fifth Assessment Report of the Intergovernmental Panel on Climate Change, Cambridge University Press, Cambridge, 2013.

Buchard, V., Randles, C. A., da Silva, A. M., Darmenov, A., Colarco, P. R., Govindaraju, R., Ferrare, R., Hair, J., Beyersdorf, A. J., Ziemba, L. D., Yu, H., Buchard, V., Randles, C. A., Silva, A. M. da, Darmenov, A., Colarco, P. R., Govindaraju, R., Ferrare, R., Hair, J., Beyersdorf, A. J., Ziemba, L. D., and Yu, H.: The MERRA-2 Aerosol Reanalysis, 1980 Onward. Part II: Evaluation and Case Studies, J. Clim., 30, 6851–6872, https://doi.org/10.1175/JCLI-D-16-0613.1, 2017.

Butt, E. W., Turnock, S. T., Rigby, R., Reddington, C. L., Yoshioka, M., Johnson, J. S., Regayre, L. A., Pringle, K. J., Mann, G. W., and Spracklen, D. V.: Global and regional trends in particulate air pollution and attributable health burden over the past 50 years, Environ. Res. Lett., 12, 104017, https://doi.org/10.1088/1748-9326/aa87be, 2017.

Checa-Garcia, R., Hegglin, M. I., Kinnison, D., Plummer, D. A., and Shine, K. P.: Historical Tropospheric and Stratospheric Ozone Radiative Forcing Using the CMIP6 Database, Geophys. Res. Lett., 45, 3264–3273, https://doi.org/10.1002/2017GL076770, 2018.

Chin, M., Diehl, T., Tan, Q., Prospero, J. M., Kahn, R. A., Remer, L. A., Yu, H., Sayer, A. M., Bian, H., Geogdzhayev, I. V., Holben, B. N., Howell, S. G., Huebert, B. J., Hsu, N. C., Kim, D., Kucsera, T. L., Levy, R. C., Mishchenko, M. I., Pan, X., Quinn, P. K., Schuster, G. L., Streets, D. G., Strode, S. A., Torres, O., and Zhao, X.-P.: Multi-decadal aerosol variations from 1980 to 2009: a perspective from observations and a global model, Atmos. Chem. Phys., 14, 3657–3690, https://doi.org/10.5194/acp-14-3657-2014, 2014.

Clifton, O. E., Paulot, F., Fiore, A. M., Horowitz, L. W., Correa, G., Baublitz, C. B., Fares, S., Goded, I., Goldstein, A. H., Gruening, C., Hogg, A. J., Loubet, B., Mammarella, I., Munger, J. W., Neil, L., Stella, P., Uddling, J., Vesala, T., and Weng, E.: Influence of Dynamic Ozone Dry Deposition on Ozone Pollution, J. Geophys. Res.-Atmos., 125, e2020JD032398, https://doi.org/10.1029/2020JD032398, 2020.

Cohen, A. J., Brauer, M., Burnett, R., Anderson, H. R., Frostad, J., Estep, K., Balakrishnan, K., Brunekreef, B., Dandona, L., Dandona, R., Feigin, V., Freedman, G., Hubbell, B., Jobling, A., Kan, H., Knibbs, L., Liu, Y., Martin, R., Morawska, L., Pope, C. A., Shin, H., Straif, K., Shaddick, G., Thomas, M., van Dingenen, R., van Donkelaar, A., Vos, T., Murray, C. J. L. and Forouzanfar, M. H.: Estimates and 25-year trends of the global burden of disease attributable to ambient air pollution: an analysis of data from the Global Burden of Diseases Study 2015, Lancet, 389, 1907–1918, https://doi.org/10.1016/S0140-6736(17)30505-6, 2017.

Colette, A., Andersson, C., Baklanov, A., Bessagnet, B., Brandt, J., Christensen, J. H., Doherty, R., Engardt, M., Geels, C., Giannakopoulos, C., Hedegaard, G. B., Katragkou, E., Langner, J., Lei, H., Manders, A., Melas, D., Meleux, F., Rouïl, L., Sofiev, M., Soares, J., Stevenson, D. S., Tombrou-Tzella, M., Varotsos, K. V., and Young, P.: Is the ozone climate penalty robust in Europe?, Environ. Res. Lett., 10, 084015, https://doi.org/10.1088/1748-9326/10/8/084015, 2015.

Collins, W. J., Lamarque, J.-F., Schulz, M., Boucher, O., Eyring, V., Hegglin, M. I., Maycock, A., Myhre, G., Prather, M., Shindell, D., and Smith, S. J.: AerChemMIP: quantifying the effects of chemistry and aerosols in CMIP6, Geosci. Model Dev., 10, 585–607, https://doi.org/10.5194/gmd-10-585-2017, 2017.

Danabasoglu, G.: NCAR CESM2-WACCM model output prepared for CMIP6 AerChemMIP, https://doi.org/10.22033/ESGF/CMIP6.10023, 2019a.

Danabasoglu, G.: NCAR CESM2-WACCM model output prepared for CMIP6 CMIP, https://doi.org/10.22033/ESGF/CMIP6.10024, 2019b.

Danabasoglu, G.: NCAR CESM2-WACCM model output prepared for CMIP6 ScenarioMIP, https://doi.org/10.22033/ESGF/CMIP6.10026, 2019c.

de Wit, H. A., Hettelingh, J.-P., and Harmens, H.: Trends in ecosystem and health responses to long-range transported atmospheric pollutants (ICP Waters Report 125/2015), available at: https://www.unece.org/fileadmin/DAM/env/documents/2016/AIR/Publications/Trends_in_ecosystem_and_health_responses_to_long-range_transported_atmospheric_pollutants.pdf (last access: 9 December 2019), 2015.

Doherty, R. M., Wild, O., Shindell, D. T., Zeng, G., MacKenzie, I. A., Collins, W. J., Fiore, A. M., Stevenson, D. S., Dentener, F. J., Schultz, M. G., Hess, P., Derwent, R. G., and Keating, T. J.: Impacts of climate change on surface ozone and intercontinental

ozone pollution: A multi-model study, J. Geophys. Res.-Atmos., 118, 3744–3763, https://doi.org/10.1002/jgrd.50266, 2013.

Dunne, J. P., Horowitz, L. W., Adcroft, A. J., Ginoux, P., Held, I. M., John, J. G., Krasting, J. P., Malyshev, S., Naik, V., Paulot, F., Shevliakova, E., Stock, C. A., Zadeh, N., Balaji, V., Blanton, C., Dunne, K. A., Dupuis, C., Durachta, J., Dussin, R., Gauthier, P. P. G., Griffies, S. M., Guo, H., Hallberg, R. W., Harrison, M., He, J., Hurlin, W., McHugh, C., Menzel, R., Milly, P. C. D., Nikonov, S., Paynter, D. J., Ploshay, J., Radhakrishnan, A., Rand, K., Reichl, B. G., Robinson, T., Schwarzkopf, D. M., Sentman, L. T., Underwood, S., Vahlenkamp, H., Winton, M., Wittenberg, A. T., Wyman, B., Zeng, Y., and Zhao, M.: The GFDL Earth System Model version 4.1 (GFDL-ESM4.1): Model 1 description and simulation characteristics, J. Adv. Model. Earth Syst., 12, e2019MS002014, https://doi.org/10.1029/2019MS002014, 2020.

Emmons, L. K., Schwantes, R. H., Orlando, J. J., Tyndall, G., Kinnison, D., Lamarque, J., Marsh, D., Mills, M. J., Tilmes, S., Bardeen, C., Buchholz, R. R., Conley, A., Gettelman, A., Garcia, R., Simpson, I., Blake, D. R., Meinardi, S., and Pétron, G.: The Chemistry Mechanism in the Community Earth System Model Version 2 (CESM2), J. Adv. Model. Earth Syst., 12, 1–21, https://doi.org/10.1029/2019ms001882, 2020.

Eyring, V., Bony, S., Meehl, G. A., Senior, C. A., Stevens, B., Stouffer, R. J., and Taylor, K. E.: Overview of the Coupled Model Intercomparison Project Phase 6 (CMIP6) experimental design and organization, Geosci. Model Dev., 9, 1937–1958, https://doi.org/10.5194/gmd-9-1937-2016, 2016.

Fagerli, H. and Aas, W.: Trends of nitrogen in air and precipitation: Model results and observations at EMEP sites in Europe, 1980–2003, Environ. Pollut., 154, 448–461, 2008.

Fiore, A. M., Jacob, D. J., Field, B. D., Streets, D. G., Fernandes, S. D. and Jang, C.: Linking ozone pollution and climate change: The case for controlling methane, Geophys. Res. Lett., 29, 25–1, https://doi.org/10.1029/2002GL015601, 2002.

Fiore, A. M., Naik, V., Spracklen, D. V, Steiner, A., Unger, N., Prather, M., Bergmann, D., Cameron-Smith, P. J., Cionni, I., Collins, W. J., Dalsøren, S., Eyring, V., Folberth, G. a, Ginoux, P., Horowitz, L. W., Josse, B., Lamarque, J.-F., MacKenzie, I. a, Nagashima, T., O'Connor, F. M., Righi, M., Rumbold, S. T., Shindell, D. T., Skeie, R. B., Sudo, K., Szopa, S., Takemura, T., and Zeng, G.: Global air quality and climate., Chem. Soc. Rev., 41, 6663–83, https://doi.org/10.1039/c2cs35095e, 2012.

Forster, P. M., Maycock, A. C., McKenna, C. M., and Smith, C. J.: Latest climate models confirm need for urgent mitigation, Nat. Clim. Chang., 1–4, https://doi.org/10.1038/s41558-019-0660-0, 2019.

Fortems-Cheiney, A., Foret, G., Siour, G., Vautard, R., Szopa, S., Dufour, G., Colette, A., Lacressonniere, G., and Beekmann, M.: A 3 °C global RCP8.5 emission trajectory cancels benefits of European emission reductions on air quality, Nat. Commun., 8, 1–5, https://doi.org/10.1038/s41467-017-00075-9, 2017.

Fowler, D., Pilegaard, K., Sutton, M. A., Ambus, P., Raivonen, M., Duyzer, J., Simpson, D., Fagerli, H., Fuzzi, S., Schjoerring, J. K., Granier, C., Neftel, A., Isaksen, I. S. A., Laj, P., Maione, M., Monks, P. S., Burkhardt, J., Daemmgen, U., Neirynck, J., Personne, E., Wichink-Kruit, R., Butterbach-Bahl, K., Flechard, C., Tuovinen, J. P., Coyle, M., Gerosa, G., Loubet, B., Altimir, N., Gruenhage, L., Ammann, C., Cieslik, S., Paoletti, E., Mikkelsen, T. N., Ro-Poulsen, H., Cellier, P., Cape, J. N., Horváth, L., Loreto, F., Niinemets, Ü., Palmer, P. I., Rinne, J., Misztal, P., Nemitz, E., Nilsson, D., Pryor, S., Gallagher, M. W., Vesala, T., Skiba, U., Brüggemann, N., Zechmeister-Boltenstern, S., Williams, J., O'Dowd, C., Facchini, M. C., de Leeuw, G., Flossman, A., Chaumerliac, N., and Erisman, J. W.: Atmospheric composition change: Ecosystems–Atmosphere interactions, Atmos. Environ., 43, 5193–5267, https://doi.org/10.1016/j.atmosenv.2009.07.068, 2009.

Gao, Y., Fu, J. S., Drake, J. B., Lamarque, J.-F., and Liu, Y.: The impact of emission and climate change on ozone in the United States under representative concentration pathways (RCPs), Atmos. Chem. Phys., 13, 9607–9621, https://doi.org/10.5194/acp-13-9607-2013, 2013.

Gettelman, A., Mills, M. J., Kinnison, D. E., Garcia, R. R., Smith, A. K., Marsh, D. R., Tilmes, S., Vitt, F., Bardeen, C. G., McInerny, J., Liu, H. L., Solomon, S. C., Polvani, L. M., Emmons, L. K., Lamarque, J. F., Richter, J. H., Glanville, A. S., Bacmeister, J. T., Phillips, A. S., Neale, R. B., Simpson, I. R., DuVivier, A. K., Hodzic, A., and Randel, W. J.: The Whole Atmosphere Community Climate Model Version 6 (WACCM6), J. Geophys. Res.-Atmos., 124, 12380–12403, https://doi.org/10.1029/2019JD030943, 2019.

Gidden, M. J., Riahi, K., Smith, S. J., Fujimori, S., Luderer, G., Kriegler, E., van Vuuren, D. P., van den Berg, M., Feng, L., Klein, D., Calvin, K., Doelman, J. C., Frank, S., Fricko, O., Harmsen, M., Hasegawa, T., Havlik, P., Hilaire, J., Hoesly, R., Horing, J., Popp, A., Stehfest, E., and Takahashi, K.: Global emissions pathways under different socioeconomic scenarios for use in CMIP6: a dataset of harmonized emissions trajectories through the end of the century, Geosci. Model Dev., 12, 1443–1475, https://doi.org/10.5194/gmd-12-1443-2019, 2019.

Glotfelty, T., He, J., and Zhang, Y.: Impact of future climate policy scenarios on air quality and aerosol-cloud interactions using an advanced version of CESM/CAM5: Part I. model evaluation for the current decadal simulations, Atmos. Environ., 152, 222–239, https://doi.org/10.1016/J.ATMOSENV.2016.12.035, 2017.

Good, P.: MOHC HadGEM3-GC31-LL model output prepared for CMIP6 ScenarioMIP, https://doi.org/10.22033/ESGF/CMIP6.10845, 2019.

Good, P., Sellar, A., Tang, Y., Rumbold, S., Ellis, R., Kelley, D., Kuhlbrodt, T., and Walton, J.: MOHC UKESM1.0-LL model output prepared for CMIP6 ScenarioMIP, https://doi.org/10.22033/ESGF/CMIP6.1567, 2019.

Griffiths, P. T., Murray, L. T., Zeng, G., Archibald, A. T., Emmons, L. K., Galbally, I., Hassler, B., Horowitz, L. W., Keeble, J., Liu, J., Moeini, O., Naik, V., O'Connor, F. M., Shin, Y. M., Tarasick, D., Tilmes, S., Turnock, S. T., Wild, O., Young, P. J., and Zanis, P.: Tropospheric ozone in CMIP6 Simulations, Atmos. Chem. Phys. Discuss., https://doi.org/10.5194/acp-2019-1216, in review, 2020.

Hajima, T. and Kawamiya, M.: MIROC MIROC-ES2L model output prepared for CMIP6 CMIP, https://doi.org/10.22033/ESGF/CMIP6.902, 2019.

Hajima, T., Watanabe, M., Yamamoto, A., Tatebe, H., Noguchi, M. A., Abe, M., Ohgaito, R., Ito, A., Yamazaki, D., Okajima, H., Ito, A., Takata, K., Ogochi, K., Watanabe, S., and Kawamiya, M.: Development of the MIROC-ES2L Earth system model and the evaluation of biogeochemical processes and feedbacks, Geosci.

Model Dev., 13, 2197–2244, https://doi.org/10.5194/gmd-13-2197-2020, 2020.

Hoesly, R. M., Smith, S. J., Feng, L., Klimont, Z., Janssens-Maenhout, G., Pitkanen, T., Seibert, J. J., Vu, L., Andres, R. J., Bolt, R. M., Bond, T. C., Dawidowski, L., Kholod, N., Kurokawa, J.-I., Li, M., Liu, L., Lu, Z., Moura, M. C. P., O'Rourke, P. R., and Zhang, Q.: Historical (1750–2014) anthropogenic emissions of reactive gases and aerosols from the Community Emissions Data System (CEDS), Geosci. Model Dev., 11, 369–408, https://doi.org/10.5194/gmd-11-369-2018, 2018.

Horowitz, L. W., Naik, V., Sentman, L. T., Paulot, F., Blanton, C., McHugh, C., Radhakrishnan, A., Rand, K., Vahlenkamp, H., Zadeh, N. T., Wilson, C., Ginoux, P., He, J., John, J. G., Lin, M., Paynter, D. J., Ploshay, J., Zhang, A., and Zeng, Y.: NOAA-GFDL GFDL-ESM4 model output prepared for CMIP6 AerChemMIP ssp370-lowNTCF, Version 20180701, Earth System Grid Federation, https://doi.org/10.22033/ESGF/CMIP6.8693, 2018.

Horowitz, L. W., Naik, V., Paulot, F., Ginoux, P. A., Dunne, J. P., Mao, J., Schnell, J., Chen, X., He, J., John, J. G., Lin, M., Lin, P., Malyshev, S., Paynter, D., Shevliakova, E., and Zhao, M.: The GFDL Global Atmospheric Chemistry-Climate Model AM4.1: Model Description and Simulation Characteristics, J. Adv. Model. Earth Syst., 12, e2019MS002032, https://doi.org/10.1029/2019MS002032, 2020.

Im, U., Christensen, J. H., Geels, C., Hansen, K. M., Brandt, J., Solazzo, E., Alyuz, U., Balzarini, A., Baro, R., Bellasio, R., Bianconi, R., Bieser, J., Colette, A., Curci, G., Farrow, A., Flemming, J., Fraser, A., Jimenez-Guerrero, P., Kitwiroon, N., Liu, P., Nopmongcol, U., Palacios-Peña, L., Pirovano, G., Pozzoli, L., Prank, M., Rose, R., Sokhi, R., Tuccella, P., Unal, A., Vivanco, M. G., Yarwood, G., Hogrefe, C., and Galmarini, S.: Influence of anthropogenic emissions and boundary conditions on multi-model simulations of major air pollutants over Europe and North America in the framework of AQMEII3, Atmos. Chem. Phys., 18, 8929–8952, https://doi.org/10.5194/acp-18-8929-2018, 2018.

Isaksen, I. S. A., Granier, C., Myhre, G., Berntsen, T. K., Dalsøren, S. B., Gauss, M., Klimont, Z., Benestad, R., Bousquet, P., Collins, W., Cox, T., Eyring, V., Fowler, D., Fuzzi, S., Jöckel, P., Laj, P., Lohmann, U., Maione, M., Monks, P., Prevot, A. S. H., Raes, F., Richter, A., Rognerud, B., Schulz, M., Shindell, D., Stevenson, D. S., Storelvmo, T., Wang, W.-C., van Weele, M., Wild, M., and Wuebbles, D.: Atmospheric composition change: Climate–Chemistry interactions, Atmos. Environ., 43, 5138–5192, 2009.

Jacob, D. J. and Winner, D. A.: Effect of climate change on air quality, Atmos. Environ., 43, 51–63, https://doi.org/10.1016/j.atmosenv.2008.09.051, 2009.

John, J. G., Blanton, C., McHugh, C., Radhakrishnan, A., Rand, K., Vahlenkamp, H., Wilson, C., Zadeh, N. T., Gauthier, P. P. G., Dunne, J. P., Dussin, R., Horowitz, L. W., Lin, P., Malyshev, S., Naik, V., Ploshay, J., Silvers, L., Stock, C., Winton, M., and Zeng, Y.: NOAA-GFDL GFDL-ESM4 model output prepared for CMIP6 ScenarioMIP, Version 20180701, Earth System Grid Federation, https://doi.org/10.22033/ESGF/CMIP6.1414, 2018.

Johnson, C. E., Collins, W. J., Stevenson, D. S., and Derwent, R. G.: Relative roles of climate and emissions changes on future tropospheric oxidant concentrations, J. Geophys. Res.-Atmos., 104, 18631–18645, https://doi.org/10.1029/1999JD900204, 1999.

Karset, I. H. H., Berntsen, T. K., Storelvmo, T., Alterskjær, K., Grini, A., Olivié, D., Kirkevåg, A., Seland, Ø., Iversen, T., and Schulz, M.: Strong impacts on aerosol indirect effects from historical oxidant changes, Atmos. Chem. Phys., 18, 7669–7690, https://doi.org/10.5194/acp-18-7669-2018, 2018.

Kirkevåg, A., Grini, A., Olivié, D., Seland, Ø., Alterskjær, K., Hummel, M., Karset, I. H. H., Lewinschal, A., Liu, X., Makkonen, R., Bethke, I., Griesfeller, J., Schulz, M., and Iversen, T.: A production-tagged aerosol module for Earth system models, OsloAero5.3 – extensions and updates for CAM5.3-Oslo, Geosci. Model Dev., 11, 3945–3982, https://doi.org/10.5194/gmd-11-3945-2018, 2018.

Kirtman, B., Power, S. B., Adedoyin, J. A., Boer, G. J., Bojariu, R., Camilloni, I., Doblas-Reyes, F. J., Fiore, A. M., Kimoto, M., Meehl, G. A., Prather, M., Sarr, A., Schar, C., Sutton, R., van Oldenborgh, G. J., Vecchi, G., and Wang, H. J.: Near-term Climate Change: Projections and Predictability. In: Climate Change 2013: The Physical Science Basis. Contribution of Working Group I to the Fifth Assessment Report of the Intergovernmental Panel on Climate Change, edited by: Stocker, T. F., Qin, D., Plattner, G.-K., Tignore, M., Allen, S. K., Boschung, J., Nauels, A., Xia, Y., Bex, V., and M. Midgley, P., Cambridge University Press, Cambridge, UK and New York, NY, USA, 2013.

Krasting, J. P., John, J. G., Blanton, C., McHugh, C., Nikonov, S., Radhakrishnan, A., Rand, K., Zadeh, N. T., Balaji, V., Durachta, J., Dupuis, C., Menzel, R., Robinson, T., Underwood, S., Vahlenkamp, H., Dunne, K. A., Gauthier, P. P. G., Ginoux, P., Griffies, S. M., Hallberg, R., Harrison, M., Hurlin, W., Malyshev, S., Naik, V., Paulot, F., Paynter, D. J., Ploshay, J., Schwarzkopf, D. M., Seman, C. J., Silvers, L., Wyman, B., Zeng, Y., Adcroft, A., Dunne, J. P., Dussin, R., Guo, H., He, J., Held, I. M., Horowitz, L. W., Milly, P. C. D., Shevliakova, E., Stock, C., Winton, M., Xie, J., and Zhao, M.: NOAA-GFDL GFDL-ESM4 model output prepared for CMIP6 CMIP, Version 20190726, Earth System Grid Federation, https://doi.org/10.22033/ESGF/CMIP6.1407, 2018.

Kuhlbrodt, T., Jones, C. G., Sellar, A., Storkey, D., Blockley, E., Stringer, M., Hill, R., Graham, T., Ridley, J., Blaker, A., Calvert, D., Copsey, D., Ellis, R., Hewitt, H., Hyder, P., Ineson, S., Mulcahy, J., Siahaan, A., and Walton, J.: The Low-Resolution Version of HadGEM3 GC3.1: Development and Evaluation for Global Climate, J. Adv. Model. Earth Syst., 10, 2865–2888, https://doi.org/10.1029/2018MS001370, 2018.

Lamarque, J.-F., Shindell, D. T., Josse, B., Young, P. J., Cionni, I., Eyring, V., Bergmann, D., Cameron-Smith, P., Collins, W. J., Doherty, R., Dalsoren, S., Faluvegi, G., Folberth, G., Ghan, S. J., Horowitz, L. W., Lee, Y. H., MacKenzie, I. A., Nagashima, T., Naik, V., Plummer, D., Righi, M., Rumbold, S. T., Schulz, M., Skeie, R. B., Stevenson, D. S., Strode, S., Sudo, K., Szopa, S., Voulgarakis, A., and Zeng, G.: The Atmospheric Chemistry and Climate Model Intercomparison Project (ACCMIP): overview and description of models, simulations and climate diagnostics, Geosci. Model Dev., 6, 179–206, https://doi.org/10.5194/gmd-6-179-2013, 2013.

Leibensperger, E. M., Mickley, L. J., Jacob, D. J., Chen, W.-T., Seinfeld, J. H., Nenes, A., Adams, P. J., Streets, D. G., Kumar, N., and Rind, D.: Climatic effects of 1950–2050 changes in US anthropogenic aerosols – Part 1: Aerosol trends

and radiative forcing, Atmos. Chem. Phys., 12, 3333–3348, https://doi.org/10.5194/acp-12-3333-2012, 2012.

Lelieveld, J., Evans, J. S., Fnais, M., Giannadaki, D., and Pozzer, a: The contribution of outdoor air pollution sources to premature mortality on a global scale, Nature, 525, 367–71, https://doi.org/10.1038/nature15371, 2015.

Li, K., Jacob, D. J., Liao, H., Shen, L., Zhang, Q., and Bates, K. H.: Anthropogenic drivers of 2013–2017 trends in summer surface ozone in China, P. Natl. Acad. Sci. USA, 116, 422–427, https://doi.org/10.1073/pnas.1812168116, 2019.

Malley, C. S., Henze, D. K., Kuylenstierna, J. C. I., Vallack, H. W., Davila, Y., Anenberg, S. C., Turner, M. C., and Ashmore, M. R.: Updated Global Estimates of Respiratory Mortality in Adults = 30 Years of Age Attributable to Long-Term Ozone Exposure, Environ. Health Perspect., 125, 087021, https://doi.org/10.1289/EHP1390, 2017.

Michou, M., Nabat, P., Saint-Martin, D., Bock, J., Decharme, B., Mallet, M., Roehrig, R., Séférian, R., Sénési, S., and Voldoire, A.: Present-day and historical aerosol and ozone characteristics in CNRM CMIP6 simulations, J. Adv. Model. Earth Syst., 12, 2019MS001816, https://doi.org/10.1029/2019MS001816, 2019.

Mortier, A., Gliss, J., Schulz, M., Aas, W., Andrews, E., Bian, H., Chin, M., Ginoux, P., Hand, J., Holben, B., Hua, Z., Kipling, Z., Kirkevåg, A., Laj, P., Lurton, T., Myhre, G., Neubauer, D., Olivié, D., von Salzen, K., Takemura, T., and Tilmes, S.: Evaluation of climate model aerosol trends with ground-based observations over the last two decades – an AeroCom and CMIP6 analysis, Atmos. Chem. Phys. Discuss., https://doi.org/10.5194/acp-2019-1203, in review, 2020.

Mulcahy, J. P., Johnson, C., Jones, C. G., Povey, A. C., Scott, C. E., Sellar, A., Turnock, S. T., Woodhouse, M. T., Abraham, N. L., Andrews, M. B., Bellouin, N., Browse, J., Carslaw, K. S., Dalvi, M., Folberth, G. A., Glover, M., Grosvenor, D., Hardacre, C., Hill, R., Johnson, B., Jones, A., Kipling, Z., Mann, G., Mollard, J., O'Connor, F. M., Palmieri, J., Reddington, C., Rumbold, S. T., Richardson, M., Schutgens, N. A. J., Stier, P., Stringer, M., Tang, Y., Walton, J., Woodward, S., and Yool, A.: Description and evaluation of aerosol in UKESM1 and HadGEM3-GC3.1 CMIP6 historical simulations, Geosci. Model Dev. Discuss., https://doi.org/10.5194/gmd-2019-357, in review, 2020.

Myhre, G., Shindell, D., Breon, F.-M., Collins, W., Fuglestvedt, J., Huang, J., Koch, D., Lamarque, J.-F., Lee, D., Mendoza, B., Nakajima, T., Robock, A., Stephens, G., Takemura, T., and Zhang, H.: Anthropogenic and Natural Radiative Forcing. In: Climate Change 2013: The Physical Science Basis. Contribution of Working Group I to the Fifth Assessment Report of the Intergovernemental Panel on Cliamte Change, edited by: Stocker, T. F., Qin, D., Plattner, G.-K., Tignore, M., Allen, S. K., Boschung, J., Nauels, A., Xia, Y., Bex, V., and M. Midgley, P., Cambridge University Press, Cambridge, UK and New York, NY, USA, 2013.

NASA Goddard Institute For Space Studies (NASA/GISS): NASA-GISS GISS-E2.1H model output prepared for CMIP6 CMIP, https://doi.org/10.22033/ESGF/CMIP6.1421, 2018.

Neal, L. S., Dalvi, M., Folberth, G., McInnes, R. N., Agnew, P., O'Connor, F. M., Savage, N. H., and Tilbee, M.: A description and evaluation of an air quality model nested within global and regional composition-climate models using MetUM, Geosci. Model Dev., 10, 3941–3962, https://doi.org/10.5194/gmd-10-3941-2017, 2017.

Neubauer, D., Ferrachat, S., Siegenthaler-Le Drian, C., Stoll, J., Folini, D. S., Tegen, I., Wieners, K.-H., Mauritsen, T., Stemmler, I., Barthel, S., Bey, I., Daskalakis, N., Heinold, B., Kokkola, H., Partridge, D., Rast, S., Schmidt, H., Schutgens, N., Stanelle, T., Stier, P., Watson-Parris, D., and Lohmann, U.: HAMMOZ-Consortium MPI-ESM1.2-HAM model output prepared for CMIP6 AerChemMIP, https://doi.org/10.22033/ESGF/CMIP6.1621, 2019.

Norwegian Climate Center (NCC): NCC NorESM2-LM model output prepared for CMIP6 CMIP historical, https://doi.org/10.22033/ESGF/CMIP6.502, 2018.

O'Neill, B. C., Kriegler, E., Riahi, K., Ebi, K. L., Hallegatte, S., Carter, T. R., Mathur, R., and van Vuuren, D. P.: A new scenario framework for climate change research: the concept of shared socioeconomic pathways, Clim. Change, 122, 387–400, https://doi.org/10.1007/s10584-013-0905-2, 2014.

O'Neill, B. C., Tebaldi, C., van Vuuren, D. P., Eyring, V., Friedlingstein, P., Hurtt, G., Knutti, R., Kriegler, E., Lamarque, J.-F., Lowe, J., Meehl, G. A., Moss, R., Riahi, K., and Sanderson, B. M.: The Scenario Model Intercomparison Project (ScenarioMIP) for CMIP6, Geosci. Model Dev., 9, 3461–3482, https://doi.org/10.5194/gmd-9-3461-2016, 2016.

Oshima, N., Yukimoto, S., Deushi, M., Koshiro, T., Kawai, H., Tanaka, T. Y., and Yoshida, K.: Global and Arctic effective radiative forcing of anthropogenic gases and aerosols in MRI-ESM2.0, Prog. Earth Planet. Sci., 7, 38, https://doi.org/10.1186/s40645-020-00348-w, 2020.

Pan, X., Chin, M., Gautam, R., Bian, H., Kim, D., Colarco, P. R., Diehl, T. L., Takemura, T., Pozzoli, L., Tsigaridis, K., Bauer, S., and Bellouin, N.: A multi-model evaluation of aerosols over South Asia: common problems and possible causes, Atmos. Chem. Phys., 15, 5903–5928, https://doi.org/10.5194/acp-15-5903-2015, 2015.

Parrish, D. D., Lamarque, J. F., Naik, V., Horowitz, L., Shindell, D. T., Staehelin, J., Derwent, R., Cooper, O. R., Tanimoto, H., Volz-Thomas, A., Gilge, S., Scheel, H. E., Steinbacher, M., and Fröhlich, M.: Long-term changes in lower tropospheric baseline ozone concentrations: Comparing chemistry-climate models and observations at northern midlatitudes, J. Geophys. Res., 119, 5719–5736, https://doi.org/10.1002/2013JD021435, 2014.

Pozzer, A., de Meij, A., Pringle, K. J., Tost, H., Doering, U. M., van Aardenne, J., and Lelieveld, J.: Distributions and regional budgets of aerosols and their precursors simulated with the EMAC chemistry-climate model, Atmos. Chem. Phys., 12, 961–987, https://doi.org/10.5194/acp-12-961-2012, 2012.

Pozzoli, L., Janssens-Maenhout, G., Diehl, T., Bey, I., Schultz, M. G., Feichter, J., Vignati, E., and Dentener, F.: Reanalysis of tropospheric sulfate aerosol and ozone for the period 1980–2005 using the aerosol-chemistry-climate model ECHAM5-HAMMOZ, Atmos. Chem. Phys., 11, 9563–9594, https://doi.org/10.5194/acp-11-9563-2011, 2011.

Provençal, S., Buchard, V., da Silva, A. M., Leduc, R., Barrette, N., Elhacham, E., and Wang, S.-H.: Evaluation of $PM_{2.5}$ surface concentration simulated by Version 1 of the NASA's MERRA Aerosol Reanalysis over Israel and Taiwan, Aerosol Air Qual. Res., 17, 253–261, https://doi.org/10.4209/aaqr.2016.04.0145, 2017.

Randles, C. A., da Silva, A. M., Buchard, V., Colarco, P. R., Darmenov, A., Govindaraju, R., Smirnov, A., Holben, B., Ferrare, R., Hair, J., Shinozuka, Y., Flynn, C. J., Randles, C. A., Silva, A. M. da, Buchard, V., Colarco, P. R., Darmenov, A., Govindaraju, R., Smirnov, A., Holben, B., Ferrare, R., Hair, J., Shinozuka, Y., and Flynn, C. J.: The MERRA-2 Aerosol Reanalysis, 1980 Onward. Part I: System Description and Data Assimilation Evaluation, J. Clim., 30, 6823–6850, https://doi.org/10.1175/JCLI-D-16-0609.1, 2017.

Rao, S., Klimont, Z., Leitao, J., Riahi, K., Van Dingenen, R., Reis, L. A., Calvin, K., Dentener, F., Drouet, L., Fujimori, S., Harmsen, M., Luderer, G., Heyes, C., Strefler, J., Tavoni, M., and Van Vuuren, D. P.: A multi-model assessment of the co-benefits of climate mitigation for global air quality, Environ. Res. Lett., 11, 124013, https://doi.org/10.1088/1748-9326/11/12/124013, 2016.

Rao, S., Klimont, Z., Smith, S. J., Dingenen, R. Van, Dentener, F., Bouwman, L., Riahi, K., Amann, M., Bodirsky, B. L., Van Vuuren, D. P., Reis, L. A., Calvin, K., Drouet, L., Fricko, O., Fujimori, S., Gernaat, D., Havlik, P., Harmsen, M., Hasegawa, T., Heyes, C., Hilaire, J., Luderer, G., Masui, T., Stehfest, E., Strefler, J., Van Der Sluis, S., and Tavoni, M.: Future air pollution in the Shared Socio-economic Pathways, Glob. Environ. Chang., 42, 346–358, https://doi.org/10.1016/j.gloenvcha.2016.05.012, 2017.

Rasmussen, D. J., Hu, J., Mahmud, A., and Kleeman, J. M.: The Ozone Climate Penalty: past, present and future, Env. Sci. Technol., 47, 14258–14266, https://doi.org/10.1021/es403446m, 2013.

Reddington, C. L., Carslaw, K. S., Stier, P., Schutgens, N., Coe, H., Liu, D., Allan, J., Browse, J., Pringle, K. J., Lee, L. A., Yoshioka, M., Johnson, J. S., Regayre, L. A., Spracklen, D. V., Mann, G. W., Clarke, A., Hermann, M., Henning, S., Wex, H., Kristensen, T. B., Leaitch, W. R., Pöschl, U., Rose, D., Andreae, M. O., Schmale, J., Kondo, Y., Oshima, N., Schwarz, J. P., Nenes, A., Anderson, B., Roberts, G. C., Snider, J. R., Leck, C., Quinn, P. K., Chi, X., Ding, A., Jimenez, J. L., and Zhang, Q.: The global aerosol synthesis and science project (GASSP): Measurements and modeling to reduce uncertainty, B. Am. Meteorol. Soc., 98, 1857–1877, https://doi.org/10.1175/BAMS-D-15-00317.1, 2017.

Reis, L. A., Drouet, L., van Dingenen, R., and Emmerling, J.: Future global air quality indices under different socioeconomic and climate assumptions, Sustain, 10, 1–27, https://doi.org/10.3390/su10103645, 2018.

Riahi, K., Van Vuuren, D. P., Kriegler, E., Edmonds, J., O'Neill, B. C., Fujimori, S., Bauer, N., Calvin, K., Dellink, R., Fricko, O., Lutz, W., Popp, A., Cuaresma, J. C., Kc, S., Leimbach, M., Jiang, L., Kram, T., Rao, S., Emmerling, J., Ebi, K., Hasegawa, T., Havlik, P., Humpenöder, F., Aleluia, L., Silva, D., Smith, S., Stehfest, E., Bosetti, V., Eom, J., Gernaat, D., Masui, T., Rogelj, J., Strefler, J., Drouet, L., Krey, V., Luderer, G., Harmsen, M., Takahashi, K., Baumstark, L., Doelman, J. C., Kainuma, M., Klimont, Z., Marangoni, G., Lotze-Campen, H., Obersteiner, M., Tabeau, A., and Tavoni, M.: The Shared Socioeconomic Pathways and their energy, land use, and greenhouse gas emissions implications: An overview, Glob. Environ. Chang., 42, 153–168, https://doi.org/10.1016/j.gloenvcha.2016.05.009, 2017.

Ridley, J., Menary, M., Kuhlbrodt, T., Andrews, M., and Andrews, T.: MOHC HadGEM3-GC31-LL model output prepared for CMIP6 CMIP, https://doi.org/10.22033/ESGF/CMIP6.419, 2018.

Schultz, M. G., Schröder, S., Lyapina, O., Cooper, O., Galbally, I., Petropavlovskikh, I., Von Schneidemesser, E., Tanimoto, H., Elshorbany, Y., Naja, M., Seguel, R., Dauert, U., Eckhardt, P., Feigenspahn, S., Fiebig, M., Hjellbrekke, A.-G., Hong, Y.-D., Christian Kjeld, P., Koide, H., Lear, G., Tarasick, D., Ueno, M., Wallasch, M., Baumgardner, D., Chuang, M.-T., Gillett, R., Lee, M., Molloy, S., Moolla, R., Wang, T., Sharps, K., Adame, J. A., Ancellet, G., Apadula, F., Artaxo, P., Barlasina, M., Bogucka, M., Bonasoni, P., Chang, L., Colomb, A., Cuevas, E., Cupeiro, M., Degorska, A., Ding, A., Fröhlich, M., Frolova, M., Gadhavi, H., Gheusi, F., Gilge, S., Gonzalez, M. Y., Gros, V., Hamad, S. H., Helmig, D., Henriques, D., Hermansen, O., Holla, R., Huber, J., Im, U., Jaffe, D. A., Komala, N., Kubistin, D., Lam, K.-S., Laurila, T., Lee, H., Levy, I., Mazzoleni, C., Mazzoleni, L., McClure-Begley, A., Mohamad, M., Murovic, M., Navarro-Comas, M., Nicodim, F., Parrish, D., Read, K. A., Reid, N., Ries, L., Saxena, P., Schwab, J. J., Scorgie, Y., Senik, I., Simmonds, P., Sinha, V., Skorokhod, A., Spain, G., Spangl, W., Spoor, R., Springston, S. R., Steer, K., Steinbacher, M., Suharguniyawan, E., Torre, P., Trickl, T., Weili, L., Weller, R., Xu, X., Xue, L., and Zhiqiang, M.: Tropospheric Ozone Assessment Report: Database and Metrics Data of Global Surface Ozone Observations, Elem. Sci. Anth., 5, 58, https://doi.org/10.1525/elementa.244, 2017.

Seferian, R.: CNRM-CERFACS CNRM-ESM2-1 model output prepared for CMIP6 CMIP, https://doi.org/10.22033/ESGF/CMIP6.1391, 2018.

Seferian, R.: CNRM-CERFACS CNRM-ESM2-1 model output prepared for CMIP6 AerChemMIP, https://doi.org/10.22033/ESGF/CMIP6.1389, 2019.

Séférian, R., Nabat, P., Michou, M., Saint-Martin, D., Voldoire, A., Colin, J., Decharme, B., Delire, C., Berthet, S., Chevallier, M., Sénési, S., Franchisteguy, L., Vial, J., Mallet, M., Joetzjer, E., Geoffroy, O., Guérémy, J., Moine, M., Msadek, R., Ribes, A., Rocher, M., Roehrig, R., Salas-y-Mélia, D., Sanchez, E., Terray, L., Valcke, S., Waldman, R., Aumont, O., Bopp, L., Deshayes, J., Éthé, C., and Madec, G.: Evaluation of CNRM Earth System Model, CNRM-ESM2-1: Role of Earth System Processes in Present-Day and Future Climate, J. Adv. Model. Earth Syst., 11, 4182–4227, https://doi.org/10.1029/2019MS001791, 2019.

Sellar, A. A., Jones, C. G., Mulcahy, J., Tang, Y., Yool, A., Wiltshire, A., O'Connor, F. M., Stringer, M., Hill, R., Palmieri, J., Woodward, S., Mora, L., Kuhlbrodt, T., Rumbold, S., Kelley, D. I., Ellis, R., Johnson, C. E., Walton, J., Abraham, N. L., Andrews, M. B., Andrews, T., Archibald, A. T., Berthou, S., Burke, E., Blockley, E., Carslaw, K., Dalvi, M., Edwards, J., Folberth, G. A., Gedney, N., Griffiths, P. T., Harper, A. B., Hendry, M. A., Hewitt, A. J., Johnson, B., Jones, A., Jones, C. D., Keeble, J., Liddicoat, S., Morgenstern, O., Parker, R. J., Predoi, V., Robertson, E., Siahaan, A., Smith, R. S., Swaminathan, R., Woodhouse, M. T., Zeng, G., and Zerroukat, M.: UKESM1: Description and evaluation of the UK Earth System Model, J. Adv. Model. Earth Syst., 11, 4513–4558, https://doi.org/10.1029/2019MS001739, 2019.

Shen, L., Mickley, L. J., and Murray, L. T.: Influence of 2000–2050 climate change on particulate matter in the United States: results from a new statistical model, Atmos. Chem. Phys., 17, 4355–4367, https://doi.org/10.5194/acp-17-4355-2017, 2017.

Shindell, D. T., Kuylenstierna, J. C. I., Vignati, E., van Dingenen, R., Amann, M., Klimont, Z., Anenberg, S. C., Muller, N., Janssens-Maenhout, G., Raes, F., Schwartz, J., Faluvegi, G., Pozzoli, L., Kupiainen, K., Höglund-Isaksson, L., Emberson, L., Streets, D., Ramanathan, V., Hicks, K., Oanh, N. T. K., Milly, G., Williams, M., Demkine, V., and Fowler, D.: Simultaneously mitigating near-term climate change and improving human health and food security, Science, 335, 183–189, https://doi.org/10.1126/science.1210026, 2012.

Silva, R. A., West, J. J., Lamarque, J. F., Shindell, D. T., Collins, W. J., Faluvegi, G., Folberth, G. A., Horowitz, L. W., Nagashima, T., Naik, V., Rumbold, S. T., Sudo, K., Takemura, T., Bergmann, D., Cameron-Smith, P., Doherty, R. M., Josse, B., MacKenzie, I. A., Stevenson, D. S., and Zeng, G.: Future global mortality from changes in air pollution attributable to climate change, Nat. Clim. Chang., 7, 647–651, https://doi.org/10.1038/nclimate3354, 2017.

Silva, R. a, West, J. J., Zhang, Y., Anenberg, S. C., Lamarque, J.-F., Shindell, D. T., Collins, W. J., Dalsoren, S., Faluvegi, G., Folberth, G., Horowitz, L. W., Nagashima, T., Naik, V., Rumbold, S., Skeie, R., Sudo, K., Takemura, T., Bergmann, D., Cameron-Smith, P., Cionni, I., Doherty, R. M., Eyring, V., Josse, B., MacKenzie, I. a, Plummer, D., Righi, M., Stevenson, D. S., Strode, S., Szopa, S., and Zeng, G.: Global premature mortality due to anthropogenic outdoor air pollution and the contribution of past climate change, Environ. Res. Lett., 8, 034005, https://doi.org/10.1088/1748-9326/8/3/034005, 2013.

Solazzo, E., Bianconi, R., Hogrefe, C., Curci, G., Tuccella, P., Alyuz, U., Balzarini, A., Baró, R., Bellasio, R., Bieser, J., Brandt, J., Christensen, J. H., Colette, A., Francis, X., Fraser, A., Vivanco, M. G., Jiménez-Guerrero, P., Im, U., Manders, A., Nopmongcol, U., Kitwiroon, N., Pirovano, G., Pozzoli, L., Prank, M., Sokhi, R. S., Unal, A., Yarwood, G., and Galmarini, S.: Evaluation and error apportionment of an ensemble of atmospheric chemistry transport modeling systems: multivariable temporal and spatial breakdown, Atmos. Chem. Phys., 17, 3001–3054, https://doi.org/10.5194/acp-17-3001-2017, 2017.

Tachiiri, K. and Kawamiya, M.: MIROC MIROC-ES2L model output prepared for CMIP6 ScenarioMIP, https://doi.org/10.22033/ESGF/CMIP6.936, 2019.

Takemura, T.: Distributions and climate effects of atmospheric aerosols from the preindustrial era to 2100 along Representative Concentration Pathways (RCPs) simulated using the global aerosol model SPRINTARS, Atmos. Chem. Phys., 12, 11555–11572, https://doi.org/10.5194/acp-12-11555-2012, 2012.

Tang, Y., Rumbold, S., Ellis, R., Kelley, D., Mulcahy, J., Sellar, A., Walton, J., and Jones, C.: MOHC UKESM1.0-LL model output prepared for CMIP6 CMIP, https://doi.org/10.22033/ESGF/CMIP6.1569, 2019.

Taylor, K. E., Stouffer, R. J., and Meehl, G. A.: An Overview of CMIP5 and the Experiment Design, B. Am. Meteorol. Soc., 93, 485–498, https://doi.org/10.1175/BAMS-D-11-00094.1, 2012.

Tegen, I., Neubauer, D., Ferrachat, S., Siegenthaler-Le Drian, C., Bey, I., Schutgens, N., Stier, P., Watson-Parris, D., Stanelle, T., Schmidt, H., Rast, S., Kokkola, H., Schultz, M., Schroeder, S., Daskalakis, N., Barthel, S., Heinold, B., and Lohmann, U.: The global aerosol–climate model ECHAM6.3–HAM2.3 – Part 1: Aerosol evaluation, Geosci. Model Dev., 12, 1643–1677, https://doi.org/10.5194/gmd-12-1643-2019, 2019.

Tilmes, S., Hodzic, A., Emmons, L. K., Mills, M. J., Gettelman, A., Kinnison, D. E., Park, M., Lamarque, J. -F., Vitt, F., Shrivastava, M., Campuzano Jost, P., Jimenez, J., and Liu, X.: Climate forcing and trends of organic aerosols in the Community Earth System Model (CESM2), J. Adv. Model. Earth Syst., 11, 4323–4351, https://doi.org/10.1029/2019MS001827, 2019.

Tørseth, K., Aas, W., Breivik, K., Fjæraa, A. M., Fiebig, M., Hjellbrekke, A. G., Lund Myhre, C., Solberg, S., and Yttri, K. E.: Introduction to the European Monitoring and Evaluation Programme (EMEP) and observed atmospheric composition change during 1972–2009, Atmos. Chem. Phys., 12, 5447–5481, https://doi.org/10.5194/acp-12-5447-2012, 2012.

Tsigaridis, K., Daskalakis, N., Kanakidou, M., Adams, P. J., Artaxo, P., Bahadur, R., Balkanski, Y., Bauer, S. E., Bellouin, N., Benedetti, A., Bergman, T., Berntsen, T. K., Beukes, J. P., Bian, H., Carslaw, K. S., Chin, M., Curci, G., Diehl, T., Easter, R. C., Ghan, S. J., Gong, S. L., Hodzic, A., Hoyle, C. R., Iversen, T., Jathar, S., Jimenez, J. L., Kaiser, J. W., Kirkevåg, A., Koch, D., Kokkola, H., Lee, Y. H., Lin, G., Liu, X., Luo, G., Ma, X., Mann, G. W., Mihalopoulos, N., Morcrette, J.-J., Müller, J.-F., Myhre, G., Myriokefalitakis, S., Ng, N. L., O'Donnell, D., Penner, J. E., Pozzoli, L., Pringle, K. J., Russell, L. M., Schulz, M., Sciare, J., Seland, Ø., Shindell, D. T., Sillman, S., Skeie, R. B., Spracklen, D., Stavrakou, T., Steenrod, S. D., Takemura, T., Tiitta, P., Tilmes, S., Tost, H., van Noije, T., van Zyl, P. G., von Salzen, K., Yu, F., Wang, Z., Wang, Z., Zaveri, R. A., Zhang, H., Zhang, K., Zhang, Q., and Zhang, X.: The AeroCom evaluation and intercomparison of organic aerosol in global models, Atmos. Chem. Phys., 14, 10845–10895, https://doi.org/10.5194/acp-14-10845-2014, 2014.

Turnock, S. T., Spracklen, D. V., Carslaw, K. S., Mann, G. W., Woodhouse, M. T., Forster, P. M., Haywood, J., Johnson, C. E., Dalvi, M., Bellouin, N., and Sanchez-Lorenzo, A.: Modelled and observed changes in aerosols and surface solar radiation over Europe between 1960 and 2009, Atmos. Chem. Phys., 15, 9477–9500, https://doi.org/10.5194/acp-15-9477-2015, 2015.

Turnock, S. T., Wild, O., Dentener, F. J., Davila, Y., Emmons, L. K., Flemming, J., Folberth, G. A., Henze, D. K., Jonson, J. E., Keating, T. J., Kengo, S., Lin, M., Lund, M., Tilmes, S., and O'Connor, F. M.: The impact of future emission policies on tropospheric ozone using a parameterised approach, Atmos. Chem. Phys., 18, 8953–8978, https://doi.org/10.5194/acp-18-8953-2018, 2018.

Turnock, S. T., Wild, O., Sellar, A., and O'Connor, F. M.: 300 years of tropospheric ozone changes using CMIP6 scenarios with a parameterised approach, Atmos. Environ., 213, 686–698, https://doi.org/10.1016/J.ATMOSENV.2019.07.001, 2019.

United Nations: Paris Agreement, 2016.

van Marle, M. J. E., Kloster, S., Magi, B. I., Marlon, J. R., Daniau, A.-L., Field, R. D., Arneth, A., Forrest, M., Hantson, S., Kehrwald, N. M., Knorr, W., Lasslop, G., Li, F., Mangeon, S., Yue, C., Kaiser, J. W., and van der Werf, G. R.: Historic global biomass burning emissions for CMIP6 (BB4CMIP) based on merging satellite observations with proxies and fire models (1750–2015), Geosci. Model Dev., 10, 3329–3357, https://doi.org/10.5194/gmd-10-3329-2017, 2017.

van Vuuren, D. P., Kriegler, E., O'Neill, B. C., Ebi, K. L., Riahi, K., Carter, T. R., Edmonds, J., Hallegatte, S., Kram, T., Mathur, R., and Winkler, H.: A new scenario framework for Climate Change

Research: scenario matrix architecture, Clim. Change, 122, 373–386, https://doi.org/10.1007/s10584-013-0906-1, 2014.

Voldoire, A.: CNRM-CERFACS CNRM-ESM2-1 model output prepared for CMIP6 ScenarioMIP, https://doi.org/10.22033/ESGF/CMIP6.1395, 2019.

Weaver, C. P., Liang, X. Z., Zhu, J., Adams, P. J., Amar, P., Avise, J., Caughey, M., Chen, J., Cohen, R. C., Cooter, E., Dawson, J. P., Gilliam, R., Gilliland, A., Goldstein, A. H., Grambsch, A., Grano, D., Guenther, A., Gustafson, W. I., Harley, R. A., He, S., Hemming, B., Hogrefe, C., Huang, H. C., Hunt, S. W., Jacob, D. J., Kinney, P. L., Kunkel, K., Lamarque, J. F., Lamb, B., Larkin, N. K., Leung, L. R., Liao, K. J., Lin, J. T., Lynn, B. H., Manomaiphiboon, K., Mass, C., Mckenzie, D., Mickley, L. J., O'Neill, S. M., Nolte, C., Pandis, S. N., Racherla, P. N., Rosenzweig, C., Russell, A. G., Salathé, E., Steiner, A. L., Tagaris, E., Tao, Z., Tonse, S., Wiedinmyer, C., Williams, A., Winner, D. A., Woo, J. H., Wu, S., and Wuebbles, D. J.: A preliminary synthesis of modeled climate change impacts on U.S. regional ozone concentrations, B. Am. Meteorol. Soc., 90, 1843–1863, https://doi.org/10.1175/2009BAMS2568.1, 2009.

Westervelt, D. M., Horowitz, L. W., Naik, V., Tai, A. P. K., Fiore, A. M. and Mauzerall, D. L.: Quantifying $PM_{2.5}$-meteorology sensitivities in a global climate model, Atmos. Environ., 142, 43–56, https://doi.org/10.1016/J.ATMOSENV.2016.07.040, 2016.

Wild, O. and Prather, M. J.: Global tropospheric ozone modeling: Quantifying errors due to grid resolution, J. Geophys. Res.–Atmos., 111, 1–14, https://doi.org/10.1029/2005JD006605, 2006.

Wild, O., Fiore, A. M., Shindell, D. T., Doherty, R. M., Collins, W. J., Dentener, F. J., Schultz, M. G., Gong, S., MacKenzie, I. A., Zeng, G., Hess, P., Duncan, B. N., Bergmann, D. J., Szopa, S., Jonson, J. E., Keating, T. J., and Zuber, A.: Modelling future changes in surface ozone: a parameterized approach, Atmos. Chem. Phys., 12, 2037–2054, https://doi.org/10.5194/acp-12-2037-2012, 2012.

Wild, O., Voulgarakis, A., O'Connor, F., Lamarque, J.-F., Ryan, E. M., and Lee, L.: Global sensitivity analysis of chemistry–climate model budgets of tropospheric ozone and OH: exploring model diversity, Atmos. Chem. Phys., 20, 4047–4058, https://doi.org/10.5194/acp-20-4047-2020, 2020.

World Climate Research Programme (WCRP): WCRP Coupled Model Intercomparison Project (Phase 6), ESGF, available at: https://esgf-node.llnl.gov/projects/cmip6/, last access: 8 September 2020.

Wu, S., Mickley, L. J., Leibensperger, E. M., Jacob, D. J., Rind, D., and Streets, D. G.: Effects of 2000–2050 global change on ozone air quality in the United States, J. Geophys. Res., 113, D06302, https://doi.org/10.1029/2007JD008917, 2008.

Wu, T., Lu, Y., Fang, Y., Xin, X., Li, L., Li, W., Jie, W., Zhang, J., Liu, Y., Zhang, L., Zhang, F., Zhang, Y., Wu, F., Li, J., Chu, M., Wang, Z., Shi, X., Liu, X., Wei, M., Huang, A., Zhang, Y., and Liu, X.: The Beijing Climate Center Climate System Model (BCC-CSM): the main progress from CMIP5 to CMIP6 , Geosci. Model Dev., 12, 1573–1600, https://doi.org/10.5194/gmd-12-1573-2019, 2019.

Wu, T., Zhang, F., Zhang, J., Jie, W., Zhang, Y., Wu, F., Li, L., Yan, J., Liu, X., Lu, X., Tan, H., Zhang, L., Wang, J., and Hu, A.: Beijing Climate Center Earth System Model version 1 (BCC-ESM1): model description and evaluation of aerosol simulations, Geosci. Model Dev., 13, 977–1005, https://doi.org/10.5194/gmd-13-977-2020, 2020.

Young, P. J., Archibald, A. T., Bowman, K. W., Lamarque, J.-F., Naik, V., Stevenson, D. S., Tilmes, S., Voulgarakis, A., Wild, O., Bergmann, D., Cameron-Smith, P., Cionni, I., Collins, W. J., Dalsøren, S. B., Doherty, R. M., Eyring, V., Faluvegi, G., Horowitz, L. W., Josse, B., Lee, Y. H., MacKenzie, I. A., Nagashima, T., Plummer, D. A., Righi, M., Rumbold, S. T., Skeie, R. B., Shindell, D. T., Strode, S. A., Sudo, K., Szopa, S., and Zeng, G.: Pre-industrial to end 21st century projections of tropospheric ozone from the Atmospheric Chemistry and Climate Model Intercomparison Project (ACCMIP), Atmos. Chem. Phys., 13, 2063–2090, https://doi.org/10.5194/acp-13-2063-2013, 2013.

Young, P. J., Naik, V., Fiore, A. M., Gaudel, A., Guo, J., Lin, M. Y., Neu, J. L., Parrish, D. D., Rieder, H. E., Schnell, J. L., Tilmes, S., Wild, O., Zhang, L., Ziemke, J. R., Brandt, J., Delcloo, A., Doherty, R. M., Geels, C., Hegglin, M. I., Hu, L., Im, U., Kumar, R., Luhar, A., Murray, L., Plummer, D., Rodriguez, J., Saiz-Lopez, A., Schultz, M. G., Woodhouse, M. T. and Zeng, G.: Tropospheric Ozone Assessment Report: Assessment of global-scale model performance for global and regional ozone distributions, variability, and trends, Elem. Sci. Anth., 6, 10, https://doi.org/10.1525/elementa.265, 2018.

Yukimoto, S., Koshiro, T., Kawai, H., Oshima, N., Yoshida, K., Urakawa, S., Tsujino, H., Deushi, M., Tanaka, T., Hosaka, M., Yoshimura, H., Shindo, E., Mizuta, R., Ishii, M., Obata, A., and Adachi, Y.: MRI MRI-ESM2.0 model output prepared for CMIP6 AerChemMIP, https://doi.org/10.22033/ESGF/CMIP6.633, 2019a.

Yukimoto, S., Koshiro, T., Kawai, H., Oshima, N., Yoshida, K., Urakawa, S., Tsujino, H., Deushi, M., Tanaka, T., Hosaka, M., Yoshimura, H., Shindo, E., Mizuta, R., Ishii, M., Obata, A., and Adachi, Y.: MRI MRI-ESM2.0 model output prepared for CMIP6 CMIP historical, https://doi.org/10.22033/ESGF/CMIP6.6842, 2019b.

Yukimoto, S., Koshiro, T., Kawai, H., Oshima, N., Yoshida, K., Urakawa, S., Tsujino, H., Deushi, M., Tanaka, T., Hosaka, M., Yoshimura, H., Shindo, E., Mizuta, R., Ishii, M., Obata, A., and Adachi, Y.: MRI MRI-ESM2.0 model output prepared for CMIP6 ScenarioMIP, https://doi.org/10.22033/ESGF/CMIP6.638, 2019c.

Yukimoto, S., Kawai, H., Koshiro, T., Oshima, N., Yoshida, K., Urakawa, S., Tsujino, H., Deushi, M., Tanaka, T., Hosaka, M., Yabu, S., Yoshimura, H., Shindo, E., Mizuta, R., Obata, A., Adachi, Y., and Ishii, M.: The meteorological research institute Earth system model version 2.0, MRI-ESM2.0: Description and basic evaluation of the physical component, J. Meteorol. Soc. Jpn., 97, 931–965, https://doi.org/10.2151/jmsj.2019-051, 2019d.

Zhang, J., Wu, T., Shi, X., Zhang, F., Li, J., Chu, M., Liu, Q., Yan, J., Ma, Q., and Wei, M.: BCC BCC-ESM1 model output prepared for CMIP6 CMIP, https://doi.org/10.22033/ESGF/CMIP6.1734, 2018.

Zhang, J., Wu, T., Shi, X., Zhang, F., Li, J., Chu, M., Liu, Q., Yan, J., Ma, Q., and Wei, M.: BCC BCC-ESM1 model output prepared for CMIP6 AerChemMIP, https://doi.org/10.22033/ESGF/CMIP6.1733, 2019.